National University of Lesotho

Energy Research Centre

Wind measurements using SODAR: Hirundo wind farms case study

Molibeli Rakauoane 201700079

A dissertation submitted in partial fulfillment
of the requirements for the degree of

Master of Science in Sustainable Energy

Offered by the

Energy Research Centre
Faculty of Science & Technology

August 2024

ABSTRACT

This study compares the wind data of the European Centre for Medium-Range Weather Forecasts Reanalysis Version 5 (ERA 5) to that obtained from the sound detection and ranging (SODAR) at the Rothe Plateau. It utilizes industry-standard software, Wind Atlas Analysis and Application Program (WAsP), to undertake the analysis. WAsP was employed to generate wind resource maps, to model the wind flow over complex topography and to forecast the yearly wind conditions. The availability of SODAR data, obtained from 23 January 2024, to 31 July 2024, after eliminating inaccurate and suspicious data, was 57.36%. It is commonly perceived as being of inferior quality due to its failure to meet the 90% threshold. The precision of wind resource validation is determined by the degree of accuracy and availability of the relevant data.

The findings of this study show that the forecast errors of ERA 5 represent about 12.2% of the range of SODAR wind speed data, indicating a moderate level of accuracy. The normalized root mean square error (NRMSE) for wind speed and direction were found to be 0.122 and 0.359, respectively. The ERA 5 provided inaccurate wind direction. Furthermore, the mean bias error (MBE) of -1.51 m/s and -7.84^0, respectively, for wind speed and direction were discovered, indicating an under prediction by the ERA 5 model. The correlation coefficient (*R*) between the two datasets was determined to be 0.725 (72.5%). Demonstrating a robust and reliable connection between SODAR and ERA 5. However, the wind direction correlation indicated a relatively poor connection of 27.7%. With a determination coefficient (R^2) of 0.525, ERA 5 is not able to capture and represent the complexity and dynamics influencing fluctuations in wind speed variations.

The chosen turbine generator for the Hirundo Energy wind farm is the Vestas V162-6.0 MW, with a maximum rated power of 6.0 MW. The wind farm contributes significantly to the generation of renewable energy, with an anticipated net annual production of 75.5 GWh, about 8.9% compared to the country's consumption of 848 GWh per annum in 2022. This proves that wind energy technology can be effectively harnessed in Lesotho and highlights the significance of data validation and farm planning for optimizing energy output and efficiency. However, due to the lack of continuous onsite measurements, the capacity factor was found to be 17.95%, compared to a global average of 30% for grid-connected wind farms.

ACKNOWLEDGEMENTS

I would like to sincerely thank Professor Moeketsi Mpholo, my main supervisor, for his valuable guidance, assistance, and knowledge throughout this research study. This research has greatly benefited from his perceptive criticism and constant support. In Addition, I would like to thank Mr. Jacob Demeyer, my co-supervisor, for his insightful advice and help in navigating the challenges of wind resource assessment. His knowledge and commitment have made this research study more valuable than it would otherwise be.

I would particularly like to thank Mr. Tšita Molapo for his great help with the SODAR device installation and operation. His technological know-how and meticulous dedication to detail were important to this project accomplishment. I also appreciate Mr. Ketso Molapo's help with the insights on ERA5 data.

Finally, I would like to express my gratitude to everyone, especially the Hirundo Energy team and the Energy Research Centre (ERC); they have supported my research endeavour in one way or another. I sincerely appreciate their help and the chance to work with such a committed group of people.

Table of Contents

List of Acronyms

ERA 5 : European Centre for Medium-Range Weather Forecasts Reanalysis Version 5

SODAR : Sound Detection and Ranging

WAsP : Wind Atlas Analysis and Application Program

NRMSE : Normalized Root Mean Square Error

MBE : Mean Bias Error

LIDAR : Light Detection and Ranging

EDM : Electricidade de Moçambique

SAPP : Southern African Power Pool

PPA : Power Purchase Agreement

IPP : Independent Power Producer

ECMWF : European Centre for Medium-Range Weather Forecasts

WRA : Wind Resource Assessment

AEP : Annual Energy Production

WS : Wind Speed

WD : Wind Direction

ABL : Above Boundary Layer

RADAR : Radio Detection and Ranging

EU WISE : European Union Wind Energy SODAR Evaluation

NREL : National Renewable Energy Laboratory

SNR : Sound to Noise Ratio

RMSE : Root Mean Square Error

MAE : Mean Absolute Error

R^2 : Determination Coefficient

R : Correlation Coefficient

σ : Standard Deviation

PV : PhotoVoltaic

FFT : Fast Fourier Transform

WACA : WAsP Climate Analyst

OMWC : Observed Mean Wind Climate

PDF : Probability Density Function

1. INTRODUCTION

1.1. Background

Renewable energy is growing in global energy production and development strategies, accounting for 29.6% of global electricity generation in 2021, a significant increase from the 19.8% generated in 2010 [1]. It provides a sustainable alternative to greenhouse gas-emitting conventional fossil fuel electricity generators. Wind energy, in particular, is becoming increasingly popular as a source of clean, green, and sustainable energy on a global level. It is the second most significant non-hydropower renewable energy source, with installed capacity rising from 197 GW in 2010 to 906 GW in 2022. Comparatively, solar energy is the most popular technology, with installed capacity increasing from 40 GW in 2010 to 1131 GW in 2022 [2, 3]. The deployment of wind energy could contribute to an aspired decrease in global warming atmospheric mean temperatures of 0.3˚C to 0.8˚C by the end of this century. Realizing that global warming should be limited to 1.5˚C over the pre-industrial levels by 2030 according to the Paris Climate Agreement [4 - 6], its potential contribution to climate mitigation cannot be underestimated. There is an anticipated increase in activity in the Western markets and Africa that will drive a compound annual growth rate of 10.1% for grid-connected wind power. This growth is expected to result in 2.38 TW of cumulative installed capacity at the end of 2032 [7].

Wind farm projects necessitate a significant amount of effort to be implemented. Site assessment and energy forecasts are critical for all the relevant parties, including investors, financiers, and developers. It is an important stage in estimating a certain site's energy production potential and, eventually, the income that it will provide [8]. Various wind resource assessment methods are utilized. One of the primary causes of inaccurate estimates of wind farm energy generation has been lack of dependable data on micro performance parameters. This is due to poor system modeling, lack of technical expertise and insufficient research and development to support wind energy initiatives [9]. Addressing these challenges is of utmost importance to ensure effective implementation of wind farm projects. It may not only promote sustainable energy generation but it also contributes to economic growth.

Wind speed, turbine placement and turbine size are just a few of the variables that affect how much energy wind farms generate overall. The higher the turbine's height above ground level, the higher the wind speeds can be reached, and the larger the rotor diameter, the better the capture of wind. The ever-increasing physical size of modern wind turbines (hub height and rotor diameter), as demonstrated in Figure 1, has resulted in hub-height wind speed mast measurements becoming prohibitively expensive [10]. Mast prices rose dramatically with height in 2018. A typical 60 m mast would cost approximately $25,000–$40,000 (M471,512.5-M754,420), while an 80 m mast would range from $80,000–$130,000 (M1,508,840-M2,451,865), and in most places, their installation requires a lengthy authorization (approximately 6 months) process for siting permits [11]. Hence, there is a need to look at alternatives. One such alternative is the ground-based SODAR system that measures wind resource parameters at multiple levels, that is simple to operate and that is economically competitive with other wind sensing systems (Light Detection and Ranging, Radio Detection and Ranging, and meteorological mast). For instance, for up to 300 m of vertical profiling, would cost $60,000–$70,000 (M1,131,630-M1,320,235) while Light Detection and Ranging (LIDAR) would cost around $175,000 (M3,300,587.5) [11].

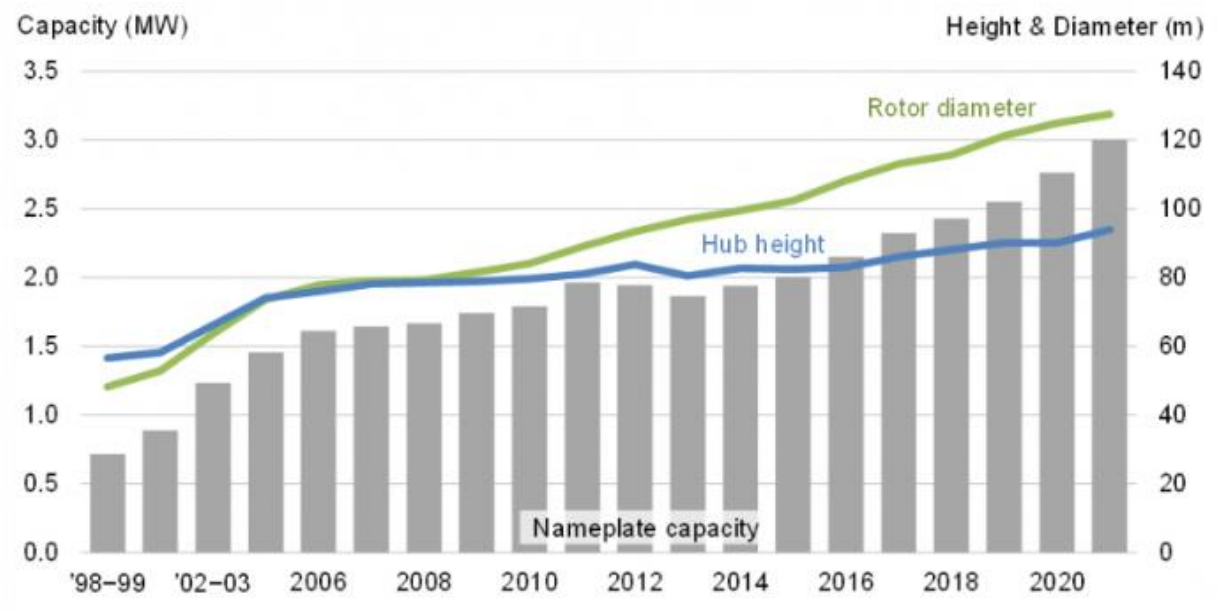

Figure 1: Trend of average turbine hub height, rotor diameter, and capacity [12]

SODAR is a remote sensing method used to measure wind properties in the atmosphere. It sends high-frequency (4000 Hz) short-pulse sound waves into the atmosphere in at least three upward directions. These waves are usually in the ultrasonic range and their reflections off air currents or aerosol particles (dust, pollen, etc.) are studied to find wind speed, direction and turbulence at different heights [13]. The scattering of sound waves by turbulent refractive index variations in the atmosphere produces a time-series signal from each direction. The spectral analysis of the time-gated portion of these time series yields a spectral peak whose frequency is an indicator of the Doppler shift that results from the moving object [14].

SODAR devices are especially effective in areas where direct measurements are difficult or limited, such as over bodies of water, and in places such as Lesotho that have diverse, complex terrain and high elevations. Lesotho has a huge potential to generate more than 6,000 MW of wind energy, especially in high-altitude areas [15]. Wind power is an appealing choice for renewable energy development due to the regular high wind speeds experienced in certain places. With average wind speeds of 5.97 m/s and 4.93 m/s at 10 m above ground and 5.5 m/s at 9 m above ground, respectively, for Letšeng, Masitise and Sani [16, 17]. Furthermore, the Global Wind Atlas reports that Lesotho has an overall mean wind speed of 10 m/s at 150 m above ground level [18]. This data helps in evaluating the feasibility of wind energy production. To properly exploit this potential, it is critical to understand the intricate local wind flow patterns of the proposed project areas, including wind speed, direction and variations at different elevations. Investing in local renewable energy projects can minimize dependence on imported electricity, which is about 507.71 GWh (63%) annually [19].

1.1. Problem Statement

In terms of energy supply security, Lesotho's grid electricity production is limited, with an installed capacity of 74.7 MW hydropower and 30 MWp of solar power [19]. The existing power facilities, with ’Muela hydropower as the main generator at 72 MW, are struggling to fulfill the rising electricity demand, particularly during peak periods. To meet Lesotho’s demand, of which the peak was 203.48 MW in 2022, up to 128.78 MW (63% of the 2022 national peak demand) of electricity is imported from Eskom in South Africa and Electricidade de Moçambique (EDM) in Mozambique through the Southern African Power Pool (SAPP) [20]. Lesotho's reliance on imports exposes the country to vulnerabilities such as variations in unit purchase prices (M/kWh)

and the availability of energy from supplier countries. As a result, there is a need to investigate the possibility of local generation from renewable energy sources, especially because Lesotho does not have any known fossil fuels.

Electricity is a critical component in driving socioeconomic development. Lesotho recognizes its importance in generating economic progress, raising living conditions, and boosting industries [21]. However, it has been determined that the low household electrification rate of 52% as of 2022, as well as reliance on imported electricity, impedes economic development [20]. When individuals lack access to electricity, they are often unable to obtain adequate food, schooling, medical care, sanitation, or other necessities for daily living, resulting in a poverty trap.

Lesotho has acknowledged the importance of renewable energy as a sustainable and clean source of electricity and plans to implement some strategies to encourage the development of renewable energy projects. This includes developing a Power Purchase Agreement (PPA) framework that will allow the participation of independent power producers (IPPs) in wind, solar, biomass, and hydropower generation [22]. Having reliable wind data provides a clear picture of the potential wind power-generating sources, which is important in developing strategies to help achieve increased energy security [23].

1.2. Research Questions and Objectives

The major goal of this research is to validate the wind measurements at Rothe Plateau using SODAR. Therefore, the main research question that this study addresses is as follows: For the selected area, how do SODAR wind measurement data and ERA 5 reanalysis data compare in terms of accuracy and reliability for wind power generation predictions?

Answers to the following sub-questions and objectives will address this question for this work:

- How does the ERA 5 reanalysis data compare to SODAR data in terms of the accuracy of wind speed and direction?
- How do the wind profiles from SODAR and ERA 5 influence the wind power generation predictions when analyzed using WAsP?

1.3. Justification

Although there has been research done on assessing potential wind resources at the identified site using ERA 5 (European Centre for Medium-Range Weather Forecasts (ECMWF) Reanalysis Version 5), validation with measurements carried out at the site itself is critical for wind farm planning, design, operation, and financial close. The SODAR wind profiler can produce comprehensive vertical wind profiles ranging from 20 m to 300 m above ground level (a.g.l) and allowing for better knowledge of wind shear, turbulence and vertical wind structure, all of which are critical for wind energy estimates [24]. Wind speeds and directions at various altitudes can affect wind turbine performance and efficiency; thus, SODAR data aids in forecasting how turbines will operate in various wind conditions, allowing developers to select suitable turbine models and to optimize their layout for a wind farm. Lesotho's complex geography includes high peaks and deep valleys, which can have a substantial impact on local wind patterns. Due to the country's complex terrain and renewable energy potential, it is essential to carry out wind measurement studies.

1.4. Report Structure

The study focuses on wind measurements with SODAR technology. The study is divided into five key chapters. The first chapter is an introduction that discusses the importance of accurate wind evaluations for wind energy applications and introduces SODAR technology as a tool for complex terrain wind profiling. The second chapter is a review of prior studies on wind assessment techniques, with an emphasis on SODAR accuracy compared to other assessment methods. The methodology is described in the third chapter; it describes the research approach, including the deployment of the SODAR equipment, data gathering procedures, data processing, and wind power generation. The results and discussion chapter follows, displaying the wind data obtained, including vertical profiles of wind speed and direction, assessing variations across different elevations and determining the associated errors. This chapter also compares SODAR data to ERA 5 data to analyze the variability in wind measurements and its effect on overall energy production forecasts. The final chapter is the conclusion. It highlights the important findings and shares relevant recommendations.

2. LITERATURE REVIEW

2.1. Overview of Wind Resource Assessment

Wind resource assessment (WRA) is the first and most significant factor to consider in the design of a wind farm. The accuracy of the wind energy resource evaluation directly determines the operating income of a wind farm when construction is complete. The wind energy resource assessment analyzes the natural features of wind energy and evaluates meteorological data from observations such as wind speed, wind direction, air temperature, air pressure and the density of the wind on the wind farm [25]. WRA is critical for the construction of wind farms and the manufacturing of wind turbines.

Wind turbine power production is determined by wind speed at the hub height and the position of each turbine, which has a direct impact on annual energy production (AEP) estimates. Furthermore, when multiple wind turbines are built at a site, the wind resource must be analyzed at each turbine location. As a result, wind resource evaluation consists of three steps: wind resource measurement, long-term resource estimation and hub height and position resource estimation [26]. As illustrated in Figure 2, the WRA can be divided into two major techniques.

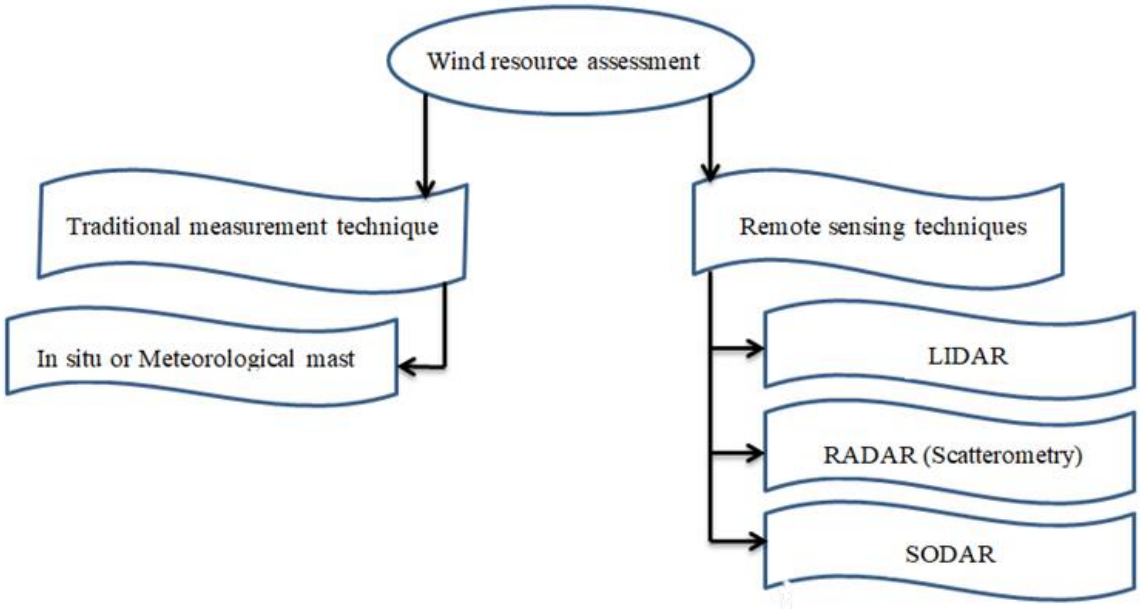

Figure 2: Classification of wind resource assessment techniques [26]

Wind resource evaluation necessitates a clear set of objectives to select the optimal assessment approach. Its eventual effectiveness is dependent on good siting and measuring methodologies, high-quality equipment and detailed data processing techniques [27].

2.2. Wind Resource Assessment Techniques

2.2.1. Meteorological Station Measurements

In-situ or meteorological station (met station) data is sufficient and most accurate for site-specific analysis; nevertheless, obtaining a lengthy duration can be challenging and expensive. This is because the measurements are acquired directly at the source, providing the most exact and true portrayal of the conditions or phenomena under investigation [28].

Sensors are utilized to quantify physical factors such as temperature, pressure and humidity. Met masts also use anemometers to measure wind speed (WS) and wind vanes to determine the wind direction (WD) [26]. The cup anemometers aerodynamic shape converts wind pressure force into rotating torque. This design ensures that the cups respond adequately to the wind force because they will fill with air as the wind blows, causing a pressure differential between the interior and outside of the cup. This pressure difference provides a force that causes the cups to rotate. The anemometer consists of a mechanism (such as gears) that transmits this rotation to an electrical sensor that records the speed of rotation by converting the mechanical motion generated by wind into an electrical signal [29]. The wind vane employs a potentiometer-type transducer that generates an electrical signal concerning the vane's position [29]. By aligning itself with the wind, the vane continually looks for a point of force equilibrium. The pointing direction of the vane indicates the wind direction. [29]

2.2.2. Remote Sensing Technology

The problems with meteorological mast measurements include the fact that it is rarely located precisely where wind turbines are built; it cannot be moved once built; cup anemometers are fixed or stationary and can only measure a relatively small fixed point at a time; it is not capable of measuring the entire area utilized by wind turbine blades [29]. Remote sensing technology addresses these challenges. It is of special importance because of the difficulty in installing masts in complex terrain as well as measuring the extremely fluctuating wind resources at different

places near wind farm facilities. It is prohibitively expensive to build numerous masts at all potential turbine sites to characterize the wind resource. However, positioning remote sensing equipment at multiple locations inside a site may be rather simple and the cost savings may be significant.

The use of various devices and sensors to obtain data regarding wind patterns, speed, direction, and other weather-related variables remotely without being in direct contact with the atmosphere is referred to as remote sensing technology. There are multiple approaches for assessing wind resources remotely; each approach has its own pros and cons. Remote sensing devices can cover large geographic areas, offering a comprehensive picture of wind resources at the regional or global level. They have the potential to minimize the need for costly and time-consuming met towers, making wind resource evaluation more cost-effective [30]. Remote sensing technology minimizes the environmental footprint of wind energy projects by reducing the requirement for physical infrastructure such as meteorological towers.

Remote sensing technologies use the Doppler Effect to detect air movement in the atmospheric boundary layer (ABL) and determine wind speed and direction [24]. These techniques provide a cost-effective method to fully depict wind patterns at suitable sites, considering the limitations and costs involved in building tall masts to reach the tip height for modern turbines (250 meters). They also serve as the only feasible approach for measuring the variation in wind speed, or shear, across the entire rotor disc of a contemporary wind turbine [24, 31]. These technologies provide extensive information regarding wind speed and direction at different altitudes while being non-intrusive in their collection of wind data. Although the data obtained from remote sensors is valuable, it is more sensitive to significant inaccuracies, such as atmospheric stability and reflections or diffractions of sound or light waves, when compared to the masts.

2.2.2.1. Light Detection and Ranging (LIDAR)

LIDAR works on the premise of emitting laser beams and monitoring the time that it takes for the beam of light to bounce off aerosol particles (water droplets, pollen, dust, etc.). The Doppler Effect is used to calculate the wind speed, and the period of flight determines the range (height) [32]. LIDAR can generate vertical profiles of wind speed and direction from 20 m up to 300 m above ground level, giving critical data for evaluating the wind resource at a given location [32]. Marti et al. conducted a study on the use of LIDARs in complex terrain in Spain [24]. They

acknowledged the utility of the technology in contrast to the installation of exceedingly tall towers in regions where access might frequently present challenges.

The Continuous Wave LIDAR is a form of LIDAR system that uses a continuous laser beam to detect distance. Due to its continuous measuring capabilities, it is well suited to capture a variety of wind conditions, detecting even minor movements or adjustments to the target environment [32]. The pulsed wave LIDAR emits brief bursts of infrared light and measures the amount of time it takes for the pulses to bounce back after reflecting off aerosol particles. The pulse has a period of hundreds of nanoseconds, which is used to compute the time frame of the pulse in the surrounding atmosphere and the spatial resolution [33]. However, Bradley found that a pulsed-laser LIDAR in complex terrain can result in horizontal wind speed inaccuracies of 5% up to 20% [34]. In general, LIDAR has demonstrated high accuracy in calculating average wind speeds and profiles in flat terrain. The data indicates that the measurements and regression slopes are close to 1, and the correlation coefficients are more than 0.99 for both LIDAR and mast measurements.

2.2.2.2. Satellite Data

Satellite data have coarser spatial and temporal resolutions than ground-based systems, making them useful for large-scale wind resource assessment and studies on climate [35]. Satellite data contributes to the building of global atlases by identifying places with high wind energy potential. Its data is integrated into predictive models for the weather to improve both short- and long-term wind forecasts, thus assisting in electricity grid oversight and storm prediction [35]. Satellite observations are used to research long-term climatic trends, such as changes in wind patterns and the effect that they have on wind energy resources.

Wind resource assessment at the regional scale necessitates spatiotemporal datasets which can be produced via satellite-derived observations and reanalysis datasets. Satellite observations and reanalysis data are indirect measures that are available on a global scale and in real time. Satellite data, on the other hand, have lesser spatial and temporal resolution than reanalysis data. In addition, sensor malfunctions, rain, clouds and other factors may interfere with satellite observations [36]. The reanalysis datasets (such as the European Centre for Medium-Range Weather Forecasts Reanalysis 5) are the most accessible and dependable long-term continuous

wind data sources. The study by Nchaba et al. [37] does provide valuable insights into the long-term austral summer wind speed trends over southern Africa. The study found 95% significant confidence level trends for reanalysis datasets over the 36-year study period at 850 hPa and 10 m. However, the study also highlights the inaccuracy of trends over the north of Lesotho up to 25^{o} S captured in the climate forecast system reanalysis at 850 hPa, as this is a high-altitude area that lies above 850 hPa.

Reanalysis validations have shown that the uncertainty in characterizing wind resources can change a lot depending on things such as the location of the site, how high it is above the ground, and whether horizontal or vertical spatial approximation methods were used in the modeling process [38]. As illustrated in Table 1, the two most used global reanalysis datasets are MERRA-2 and ERA 5, with a temporal output frequency of one hour. The MERRA 2 reanalysis from NASA's Global Modeling and Assimilation Office, as well as its predecessor, MERRA, have been widely employed in the wind sector [39]. It served as one of the earliest reanalysis methods to generate data at an hourly resolution and produce winds not just at 10 m but also at 50 m above ground level. The European Centre for Medium-range Weather Forecasts (ECMWF), which is a part of the Copernicus Climate Change Service, generates the ERA 5 reanalysis. It has been gradually released since 2017 and is, by far, more wind-power-friendly than its previous version, ERA-Interim, with 1-hour resolution versus 6 hours, wind at 100 m rather than just 10 m, and a tighter horizontal grid spacing of around 30 km versus about 80 km. ERA5 is already being used for energy applications. It outperforms earlier reanalyzes. According to Olauson [40], however, ERA5 underestimates wind speeds which may result in a significant miscalculation of wind energy generation, particularly in locations with complex topography.

Table 1: Information on Global spatial coverage numerical datasets [40]

	ERA 5	**MERRA-2**
Developer	ECMWF	NASA GMAO
Temporal coverage	1950 - present	1980 - present

Temporal Output Frequency	1 hour	1 hour
Horizontal Grid Spacing	0.25˚	0.5˚ × 0.625˚
Vertical wind speed heights	10 m, 100 m	10 m, 50 m

2.2.2.3. Sound Detection and Ranging (SODAR)

SODAR is a ground-based remote sensing technology used to monitor wind profiles in the Earth's atmosphere that has been used commercially in the wind industry since the late 1980s for a variety of purposes, including micro-siting, WRA and wake measurement [24]. SODAR technology determines atmospheric parameters by transmitting and receiving high-frequency sound waves with frequencies of up to 4000 Hz (acoustic signals).

The device can identify the altitude of the reflecting atmospheric layer by evaluating the time difference between transmission and reception. One or more transmitters and several receivers are usually used; it was established that the filtering of the results and the method of calibration used were the key challenges for SODARs being employed for wind energy applications [24]. In 2005, the EU WISE project looked into SODAR tools used in wind energy and found a way to calibrate them. They also found the main reasons for measurement errors which made people in the wind energy industry more confident in the method [41]. Except at higher wind speeds (>11 m/s), there was no difference in the root-mean-square residuals of SODAR-mast and mast-mast data.

Using a transmitter and receiver that are tens of meters apart, the bistatic SODAR explores the atmosphere. However, adopting bistatic phased array SODAR systems may present hurdles in terms of system complexity and calibration. The interpretation of data from such systems necessitates complex algorithms and modeling techniques. The monostatic phased array SODAR systems use an array of transceivers placed in a single square transducer framework that serves the dual purpose of transmitting and receiving acoustic waves. Furthermore, the mono-static

SODAR with multiple independent antennas employs three or more transceivers to create sound noise and to record the backscattered sound signal [42].

The antennas are set up in such a way that the three components of the wind can be captured using a multi-beam [26]. According to a study by the National Renewable Energy Laboratory (NREL) in moderately difficult topography, the data from a met mast (80 m) and Triton SODAR showed a correlation for wind speed and wind direction up to 80 m. The study revealed a 2% difference between average wind speeds [43]. Another project was conducted in China to compare the data collected from a mast and Triton SODAR. The results showed that the availability of the data collected from the SODAR was 94.4% at a height of 70 m and 83.8% at 100 m [44]. Table 2 summarizes the benefits and drawbacks of wind resource assessment techniques.

Table 2: Overview of all wind resource assessment techniques [45].

Technique	**In-situ**	**LIDAR**	**Satellite**	**SODAR**
Coverage area	10–300 m above ground	50–200 m above ground	Regional and Global scale	10–300 m above ground
Cost	Very high	25% more costly than SODAR	Very high	$60k (M1,093,614)
Accuracy	High in complex and flat terrains	Low in complex terrains	Low resolution	Low in complex and flat terrains (External noise and barriers can lead to inaccuracies.)
Error (%)	<1%	Up to 6%	can reach 30%	>6%

2.2.2.3.1. REMTECH PA-XS SODAR

REMTECH phased array Doppler SODARs provide continuous measurements of wind speed and direction, vertical motions, turbulence, thermal structure and mixing depth [46]. These measurements are taken at heights ranging from 10 to 300 meters, depending on the specific system. The measurements are conducted by generating a robust acoustic pulse within the audio frequency range and quantifying the Doppler frequency shift of the reflected echo that returns. Thermal turbulence in the atmosphere is what causes the backscattered echo signal. The frequency content of the returning signal is analyzed to determine wind speed and direction. Equation 1 provides the wind speed from the signal that a SODAR transmits, which is a traveling wave with components (v, u).

$$WS = \sqrt{(v)^2 + (u)^2} \qquad \text{Equation 1}$$

and Equation 2 gives the wind direction [26].

$$WD = tan^{-1}\left(\frac{v}{u}\right) \qquad \text{Equation 2}$$

Where u and v are wind speed components representing the zonal wind and meridional wind, respectively.

SODARs, which are made up of three or more beams at varying angles to the vertical, can generate a three-dimensional vertical wind profile. The device effectively eliminates any unwanted signals and removes data that is considered unreliable due to background noise, enabling it to generate accurate data even in a noisy environment with minimal data averaging time. This prevents the analysis of inaccurate information. No further data processing is required to achieve the full accuracy of the system [47]. The stored data can be promptly processed to provide comprehensive statistical data summaries and climatological investigations.

The weather has a significant impact on the SODAR signal quality. A fixed echo, temperature, and humidity fluctuations in the atmosphere may have an impact on the speed and dispersion of the sound waves, thus affecting signal transmission and reception accuracy. The SODAR data that is considered quality is anything above 90% availability of the collected and processed data [45]. The signal-to-noise ratio (SNR) is an important statistic for determining the quality of SODAR signals [14]. A greater SNR suggests that the signal is stronger and more detectable

against background noise. Instrument sensitivity, environmental noise and interference can all have an impact on the SNR and, as a result, the quality of SODAR signals [48].

Bradley et al. stated that SODAR (AQ500 SODAR and Metek SODAR) measurements were regarded as highly accurate when the determination coefficient (R^2) value fell within the range of 0.975 to 0.985. There is a significant correlation between the SODAR data and reference measurements such as those obtained from a cup anemometer. The investigation revealed that the wind speed measurements obtained from the SODAR and the cup anemometer differed by approximately 5% to 6% [49]. Kelley et al. found that high-resolution pulsed Doppler LIDARs are about as roughly accurate as SODARs, with R^2 values between 0.992 and 0.997 and standard deviations between 0.31 and 0.50 m/s [46].

2.3. Error Metrics and Statistical Significance

No matter how carefully the measurements are taken, they are subjected to errors, resulting in a measured value that differs from the true value. Moreover, different methods/technologies for taking measurements introduce different error margins. This uncertainty is quantified when estimating wind resources to properly understand how and why a particular model may be underperforming. When analyzing the time series data, the model error can be separated into two components: bias and random error. The bias represents the difference between the mean observed value and the true value, while the random error quantifies the variability or the spread of the data around the model expected values.

Metrics such as root-mean-square-error (RMSE) and mean absolute error (MAE) account for both bias and random error components. RMSE or MAE can be decomposed into a bias component and a "centered" or "unbiased" component to attribute model error to bias and random error separately. The RMSE is used to assess variations between actual and modeled data, which are referred to as residuals. The RMSE is a statistics used to analyze the model performance and to estimate accuracy by quantifying the difference between model values and real observations; It is described through Equation 3 and Equation 5 [50].

$$RMSE^2 = Bias^2 + NRMSE^2 \qquad \text{Equation 3}$$

NRMSE denotes the normalized *RMSE*. Equation 4 determines the bias (mean bias error) component:

$$MBE = \frac{1}{N}\sum_{n=1}^{N}(P_n - \omega_n) \quad \text{Equation 4}$$

Where N represents the number of observations, the ω represents the observations, and p represents the predicted estimates.

$$RMSE = \left[\frac{1}{N}\sum_{n=1}^{N}(p_n - \omega_n)^2\right]^{\frac{1}{2}} \quad \text{Equation 5}$$

It can be shown that the *NRMSE* is calculated using Equation 6.

$$NRMSE = \left[\frac{1}{N}\sum_{n=1}^{N}[(p_n - \bar{p}) - (\omega_n - \bar{\omega})]^2\right]^{\frac{1}{2}} \quad \text{Equation 6}$$

The correlation coefficient (R) is another important performance metric that assesses the "correspondence" or "pattern" between two variables and is defined by Equation 7

$$R = \frac{\frac{1}{N}\sum_{n=1}^{N}(p_n - \bar{p}) - (\omega_n - \bar{\omega})}{\sigma_p \sigma_\omega} \quad \text{Equation 7}$$

Where σ_p and σ_ω are the standard deviations of the forecasts (predictions) and observations, respectively. The correlation coefficient, R, has a maximum value of 1, indicating a perfect correlation, and a minimum value of -1, which indicates a perfect negative correlation. The determination coefficient (R^2), which has the maximum and lowest values of 1 and 0, respectively, is commonly used to characterize connections when there are several independent variables. Equation 8 shows R^2, which measures the relationship between variables, specifically how independent factors influence dependent variables. This metric, which indicates how dependent variables change when only one independent variable is changed, is frequently used to differentiate between independent and dependent variables as well as to characterize the relationships between independent variables. The better model will have a low RMSE and a high R^2 [50].

$$R^2 = \left[\frac{\frac{1}{N}\sum_{n=1}^{N}(p_n - \bar{p}) - (\omega_n - \bar{\omega})}{\sigma_p \sigma_\omega}\right]^2 \quad \text{Equation 8}$$

The standard deviation is defined in Equation 9 as a measure of how much variation or dispersion there is in a group of data. A low standard deviation indicates that the values in the set

are closely clustered around the average, while a big standard deviation indicates that the values are spread out over a broader range [51].

$$\sigma = \left[\frac{\sum_{n=1}^{N}(p_n - \bar{p})^2}{N-1}\right]^{\frac{1}{2}} \quad \text{Equation 9}$$

The Earth-mover's distance (EMD) measures the variation between two distributions. It is also known as the Wasserstein distance. This metric is defined as the area between two cumulative distribution functions and can be viewed as the quantity of "dirt" required to move from one probability distribution to another to make them equal. The EMD metric has the distinct advantage of accounting for scenarios where two distributions have the same bias but differ in shape. Table 3 summarizes the major performance metrics used in the wind industry for modeling wind resource validation.

Table 3: Performance metrics for modeled wind resource validation [52]

Name	**Abbreviation**	**Description**
Bias	Bias	Difference between the mean modeled and observed result
Root mean square error	*RMSE*	It quantifies the average size of the mistakes, considering both the variability and the systematic deviation.
Normalized root mean square error	*NRMSE*	The random error part shows the changes in model variations around the mean after bias is taken out.
Correlation coefficient	*R*	Indicates the degree of similarity between the measurements of variables in a dataset.
Determination coefficient	R^2	The correspondence or pattern between the modeled and observed variable

Earth-mover's distance	*EMD*	Difference between the probability distributions between the modeled and observed variable
Mean absolute error	*MAE*	It assesses the accuracy of predictions by finding the average of the absolute differences between the projected values and the observed values.

2.4. Validation of Wind Resources

The validation of wind resources is based on statistical evaluations of wind speed, direction, turbulence and other factors. It employs error metrics such as bias, root mean square error (RMSE), normalized root mean square error (NRMSE), mean absolute error (MAE), and correlation coefficient (*R*) defined in Table 3 [53]. The degree of accuracy and availability of the data determine the precision of wind resource validation. Furthermore, the existence of complicated terrain, such as mountains or valleys, can dramatically impact wind patterns; therefore, correct validation in such places necessitates knowledge of the local or regional landscape and its influence on wind flow [54].

Major wind resource validation studies are summarized below to demonstrate the different statistical evaluations employed in comparing wind measurement methods and verifying wind models. More than 90% of the correlations are negative from -1 to 0, indicating that the predicted mountain wave effect on hub-height wind speed is not in phase with the data. However, from 0 to 1 hour, this trend is significantly flipped, with approximately 75% being positively associated [54]. Furthermore, for each occurrence, there is at least one statistically significant positive connection at the 93% confidence level.

Ramon et al. [55] examined wind speeds derived from reanalysis data using 77 meteorological towers located worldwide. The towers had measurement heights ranging from 18 m to 122 m. Median seasonal bias ranging from 0 to -1 m/s were found, along with correlation values of approximately 0.8 for ERA 5. Kalverla et al. [56] analyzed data from 27 m to 315 m across the North Sea and found that ERA 5 underestimates the recorded wind speed by approximately 0.5 m/s over the vertical wind speed profile.

Dubov et al. conducted a study that compared traditional ways of measuring wind and Doppler SODAR systems for remote sensing. They found that SODAR systems are more reliable than masts in cold temperatures, especially those near or below 0 °C, because they do not get affected by icing [57]. These characteristics make them well-suited for regions such as Lesotho, where winter temperatures fluctuate around freezing point. During the study, SODAR data availability at 100 m was around 96.93%, with a target of 97% for the entire measuring campaign. The availability of the top anemometer, on the other hand, was low at only 88.9%, due to icing incidents. There was a slight disparity in the calculated wind speed from the mast (6.22 m/s) and from the SODAR device (6.07 m/s) [57]. SODAR demonstrated equivalent uncertainty to conventional anemometry. The conclusion is that SODAR can be considered a legitimate stand-alone method for wind resource estimates, particularly given the industry preference for greater hub heights.

In another set of analysis, as demonstrated in Figure 3 for 80 m, SODAR wind speeds are slightly lower than equivalent meteorological tower speeds. Upon the application of all the filters, a total of 13,511 data points, which account for 47.4% of the total, were utilized to calculate the average wind speeds for correlation. The meteorological tower measured a mean wind speed of 10.43 m/s, whereas the SODAR measured a mean wind speed of 10.22 m/s. This results in a tower-to-SODAR ratio of 1.021. The correlation of wind direction data from the Triton SODAR and meteorological tower, on the other hand, was good, with a maximum direction error of less than 60°. There were a few observations with an error above 40° [43]. According to Zhang et al. [58], the linear regression slope between the SODAR and the cup anemometer from the automatic weather station at 270 m above reference ground level is 0.96, with a correlation coefficient of 0.963. There was a linear regression slope of 0.94 between the SODAR and the propeller anemometer from the mast at 50 m above reference ground level. There was also a correlation coefficient of 0.966 hence, the small errors were found to be acceptable.

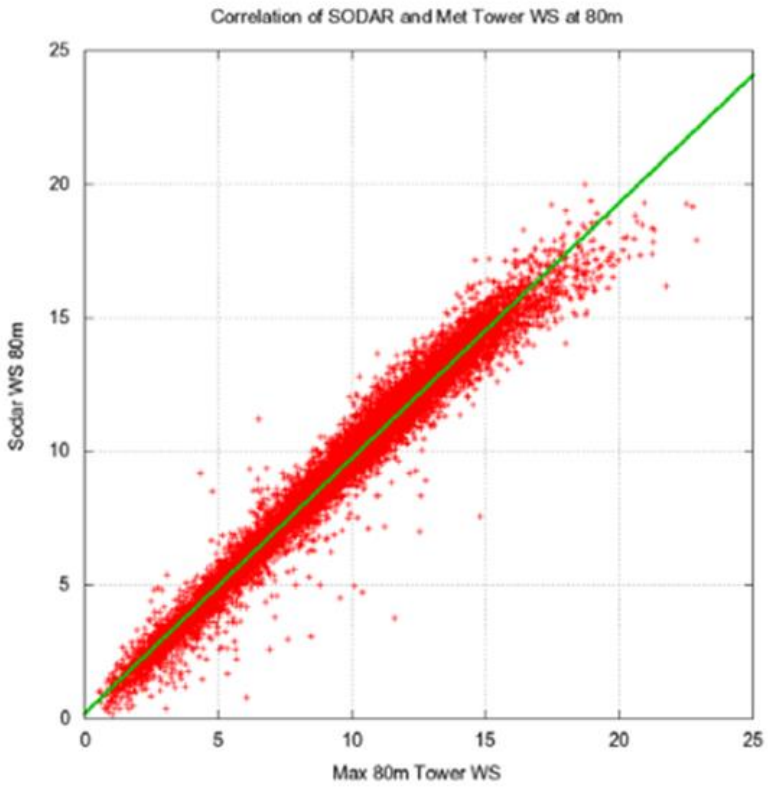

Figure 3: Comparison of wind speed measurements at 80 meters above ground level [43].

According to Shestakova et al. [59], the wind speed data from ERA 5 at a height of 100 m was compared against data from four SODARs (acoustic profilers) placed in different climate and vegetation zones across Russia. Most sites had a systematic error; ERA 5 tends to overestimate wind speed in forests and underestimate it in grasslands and deserts. The relative wind speed error was 45% at an observation point on the mountain coast. Table 4 highlights the error metrics used for validation, the results that were obtained when comparing the technologies used, and their limitations.

Table 4: Summarizing the related works

Reference	**Method**	**Evaluation criteria**	**Findings**	**Limitations**
[50]	The three methods used to	RMSE	The standard deviation	Limitations in conducting

	estimate Weibull parameters were mean measurement (MM), evaluation of measurement and justification (EMJ), and standard deviation of measurements (STDM).	R^2	for RMSE and R^2 is 0.0002 and 0.0008, respectively	accurate wind resource analysis
[42]	Validation of measurements for wind power using SODAR	R^2	The cup anemometer and the SODAR profile result in a high correlation (R^2 = 0.999)	SODAR use should be restricted for the time being because it is unable to measure high wind speeds (over 15 m/s), which impacts the wind speed distribution.
[53]	Validation of the medium-range and sub-seasonal forecast of solar irradiance and wind power using ECMWF	RMSE MAE MBE	RMSE = 4.32 MAE = 3.58 MBE = 1.21	Numerical weather prediction (NWP) methods fail to offer bias-free forecasts of 10 m wind speed for short lead times.
[60]	Comparing wind energy potential assessment using reanalysis data with the met mast	rMAE rRMSE	rMAE = 33.57% rRMSE = 49.22%	A single year's worth of measured wind data for the chosen region is not available.
[40]	An assessment of the performance of ERA5, MERRA-2, COSMO-REA6, NEWA, and AROME in simulating wind power generation.	R^2	The ERA5 dataset has robust correlations, often exceeding 0.9, except for mountainous regions, where the correlation drops below 0.77.	ERA5 underestimates wind speeds, which may result in a significant miscalculation of wind energy generation, particularly in locations with complex topography.
[48]	Characterizing coastal wind	RMSE	RMSE = 029 m/s	There have been very few, if

	energy resources using data from SODAR and microwave radiometer observations.	R^2	R^2 = 0.92	any, wind energy studies that have taken into account temperature effects based on field measurements.
[58]	SODAR, propeller anemometers, and automatic Weather Station cup anemometers were used to analyze wind characteristics and wind energy potential in a complicated hilly environment in southwest China.	R^2	R^2= 0.966 for SODAR and propeller anemometer at 50 m R^2= 0.963 for SODAR and automatic weather station cup anemometer at 272 m	Small number of observation points. More observation points are to be set up in the hilly areas of western China so that a lot more data can be collected.
[59]	Relevance of ERA 5 Reanalysis for wind Energy Applications: Comparison with SODAR Observations	Bias MAE *R* NRMSE	For four SODARs at different roughnesses and terrains: Bias = -5 - 3.8 m/s MAE = 1.4 - 2.2 m/s *R* = 0.2 - 0.98 m/s NRMSE = 0.4 - 0.8	There were no readings of wind at 100 meters in southern European Russia during the winter, when wind speed was supposed to be at its highest.

2.5. Wind Power Generation

The potential wind power that can be utilized is determined by the principles of fluid dynamics and energy conversion. The power output of a wind turbine is directly proportional to the air density (ρ) and the cube of wind speed (v). Thus, even a minor escalation in wind speed can lead to a substantial enhancement in power production [61]. Equation 10 is the kinetic energy (*KE*),

which demonstrates the relationship between the energy content of flowing air and its speed. Wind's kinetic energy is harnessed to produce electricity by converting it into mechanical energy using turbines. The turbine generator harnesses this energy and transforms it into electrical energy [61].

$$KE = \frac{1}{2}mv^2 \qquad \text{Equation 10}$$

Where *m* is the mass and *v* is the wind speed.

The wind turbine rotor blades receive the kinetic energy from the incident wind, which has mass and density and is flowing at speed *v* in the axial direction. The swept area (*A*) of the rotor blades and the wind power (P_v) can be represented using Equation 11, which demonstrates that the air density, the area that the blades cover and the wind speed raised to the power of three all affect the power that the wind produces. Nevertheless, as per the Betz limit, a theoretical boundary established by Albert Betz, it is not feasible for any wind turbine to harness more than 60% of the wind kinetic energy [62]. This is because a certain amount of wind needs to continue moving to facilitate the flow of wind through the turbine site. The maximum power output of a wind turbine, taking into account the efficiency restriction, can be calculated using Equation 12. The maximum theoretical power coefficient of the rotor C_p according to the Betz limit is 0.5926 [62].

$$P_v = \frac{1}{2}\rho A\overline{v^3} \qquad \text{Equation 11}$$

$$P_{max} = \frac{1}{2}C_p\rho A\overline{v^3} \qquad \text{Equation 12}$$

The power curve in Figure 4 illustrates the connection between wind speed and the amount of power that a wind turbine produces, beginning at the cut-in wind speed (3 m/s) required for the turbine to start generating electricity until the wind speed reaches the cut-out at which the turbine stops to operate to prevent any potential harm to the turbines [63]. The curve is defined by three points: the cut-in speed, the rated output speed and the cut-out speed. As the speed of the wind increases, the power output increases significantly, following the cubic connection described in Equation 11 until it reaches the rated speed. Any further rise in wind speed does not result in an increase in power production; it remains constant. It is important to optimize turbine positioning and to ensure a secure operation within the turbine design constraints so that the turbine stops

operating at the cut-out speed, which is typically around 25 m/s. This prevents any potential damage from high wind forces.

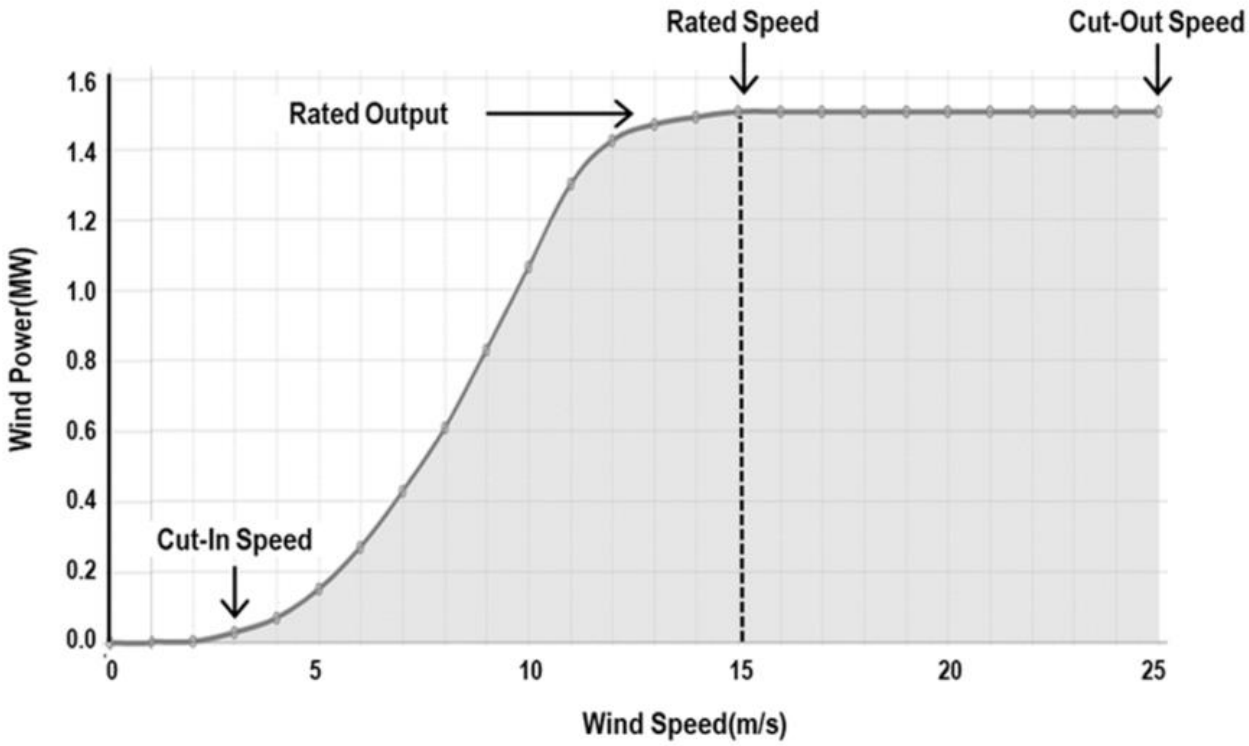

Figure 4: Wind turbine power output curve [63].

2.5.1. Air Density

Air density ρ is the quantification of the amount of air mass m present in a given volume V. Air fundamental property fluctuates in response to alterations in temperature, pressure and humidity. When the temperature of the air increases, it expands, causing a drop in density since the same amount of mass fills a larger space. In contrast, colder air undergoes contraction, leading to an increased density due to the same mass being confined within a reduced volume, as shown by Equation 13. In addition, the density of air drops as altitude increases as a result of reduced atmospheric pressure.

$$\rho = \frac{m}{V} \qquad \text{Equation 13}$$

According to the ideal gas law, the interaction between atmospheric pressure (p), atmospheric temperature (T in Kelvin), and the specific gas constant ($R = 287\ J/kgK$) for dry air determines

air density [64]. Atmospheric pressure is given by Equation 14 and can be rearranged to calculate air density, as shown by Equation 15. When temperature rises or pressure drops, the density of air reduces but, conversely, when temperature drops or pressure increases, the density of air increases. Air density is crucial for the design and functioning of wind turbines as it directly impacts the aerodynamic forces and the efficiency of energy conversion [64].

$$p = \rho RT \qquad \text{Equation 14}$$

$$\rho = \frac{p}{RT} \qquad \text{Equation 15}$$

2.5.2. Weibull Distribution Function

The Weibull distribution function is used to analyze the fluctuations in wind speed over a period of time, assisting in determining the potential for wind energy at a particular location. Equation 16 shows the probability density function of the Weibull distribution.

$$f(v) = \left(\frac{k}{c}\right)\left(\frac{v}{c}\right)^{k-1} e^{-\left(\frac{v}{c}\right)^{k}} \qquad \text{Equation 16}$$

Where v represents the wind speed, k is the shape parameter, and c is the scale parameter. k characterizes the distribution's shape, showing whether the wind speed is more uniform or more fluctuating. Utilizing the Weibull distribution to analyze wind speed data allows for the strategic placement of wind turbines and an acceptable accuracy estimation of energy generation [65].

2.5.3. Roughness

Wind turbines are positioned at an altitude above ground level (a.g.l) to reduce the amount of air disturbance caused by ground roughness obstacles such as buildings and tall trees. The obstacles have an impact on the speed and direction of the wind. As part of the wind farm design, roughness height is taken into consideration. The logarithmic law method displayed in Equation 17 shows how the wind speed at the reference height can be determined. In Equation 18, the roughness height Z_0 is used to characterize the roughness height using the preceding equation [66].

$$V(Z_R) = V(Z)\frac{ln\left(\frac{Z_R}{Z_0}\right)}{ln\left(\frac{Z}{Z_0}\right)} \qquad \text{Equation 17}$$

$$Z_0 = exp\left(\frac{V(Z_R)ln(Z) - V(Z)\ln(Z_R)}{V(Z) - V(Z_R)}\right)$$ Equation 18

Where *V(Z)* is the velocity at any height *Z*, the speed at a reference height Z_R is $V(Z_R)$.

If the site's roughness height is not known, the power law equation displayed in Equation 19 can be utilized to calculate the desired wind speed at a particular height. The shear coefficient (m), which varies between 0 and 1, can be empirically estimated based on atmospheric stability [66].

$$(Z) = V(Z_R)\left(\frac{Z}{Z_R}\right)^m$$ Equation 19

At lower elevations, the logarithmic law yields more precise forecasts of the average wind speed, whereas the power law delivers superior outcomes for higher elevations. To obtain the most precise estimation of the average wind speed at a specific turbine height, it is generally necessary to employ both approaches and then compare the results [66].

2.5.3.1. Turbulence Intensity

The location's roughness, which is a result of the presence of vegetation, buildings, upstream turbines, and other barriers such as the terrain, is what causes the turbulence in the air. It is an unstable flow of air that leads to an increase in heat transmission and dissipation [67]. When designing a wind farm, obstacles that are located in the vicinity of the area of study have to be taken into account. In addition, the turbines should be properly spaced apart to minimize the amount of turbulence that is experienced by downstream wind turbines. Equation 20 provides the turbulence intensity.

$$TI = \frac{\sigma}{V}$$ Equation 20

Where σ is the standard deviation of the wind speed fluctuations and V is the mean wind speed.

2.5.4. Capacity Factor

The capacity factor is a measure for evaluating the effectiveness and productivity of a wind energy system. The measurement of a wind farm capacity factor compares the actual energy that it produced over a specific time period to the maximum potential energy that it may have

generated if it had been operating continuously at full capacity during that same time period, as demonstrated in Equation 21 [68].

$$CF = \frac{AEP_{net}}{Maximum\ power\ output \times Time} \quad \text{Equation 21}$$

2.6. Synthesis of the Literature

There is uncertainty over the reliability and accuracy of wind estimates conducted with remote sensing technology, particularly in non-flat (complex) terrain. Developing new instruments and ways to process data is the key step toward building trust in remote sensing [24]. As a result, the PA-XS REMTECH SODAR, is used in this work. SODAR is of particular importance in upland terrain due to the difficulties of installing masts there as well as the wind resources being extremely changeable at different positions surrounding wind farm facilities. It is prohibitively expensive to build numerous masts in various areas to accurately describe the wind resource. However, positioning remote sensing equipment at multiple locations inside a site may be rather simple, and the associated cost savings may prove to be significant.

This study seeks to investigate SODAR wind measurements on complex terrain, which are more typical of the places where the majority of modern wind turbines are erected due to their high wind potential. While many investigations on SODAR technology have been undertaken in flat terrains, this study focuses on its efficacy in highland terrains. Several wind assessment studies in Lesotho have been undertaken using reanalysis datasets [17, 61]. There are several validations of models that simulate wind resources, but they mainly focus on heights close to the ground (less than 10 m) [70]. The root mean square error (RMSE), which has been in use for a long time in the wind energy industry, is a regularly used metric for examining time series forecasts [50, 51]. However, because of the inclusion of the arithmetic mean, the RMSE is not resistant or robust. It is critical to use the correct error measures when assessing wind resources. An incorrect error metric does not only impact model optimization but may also influence model judgment. When a wind power prediction fails to predict power changes for a short period, which frequently occurs during ramp events, the forecast RMSE, mean squared error (MSE) and mean absolute error (MAE) may be excessively inflated due to its nonresistance to outliers. This is because RMSE and MSE-based measures tend to over-penalize significant errors and are hence unsuitable for ramp forecasting evaluation [73]. Researchers have used RMSE variants

such as normalized RMSE and unbiased RMSE to address RMSE's shortcomings [74]. On the other hand, while the bias should be low, there is no assurance of the data validity considering that a bias may be low for the wrong reason [51].

The correlation coefficient R is important in verifying reanalysis datasets because it represents the degree of significance of the linear connection between two variables [36]. The correlation coefficient R, the determination coefficient R^2, the mean bias error (MBE), the normalized RMSE and the standard deviation (σ) were used in this study to assess the accuracy of wind speed readings from long-term reanalysis datasets with SODAR data.

3. METHODOLOGY

3.1. Site Assessment

The wind measurements were conducted on the Rothe Plateau, located at a distance of 1,668.77 m from Masite village in the Maseru district. The terrain in the area is semi-complex (upland). The elevation of the landscape is approximately 2,042 m above sea level. The survey lasted for six months. The SODAR PA-XS system, built by the French company, REMTECH, was used to measure wind speed (WS), direction, temperature, and pressure. The measurements were taken on the Rothe Plateau, located at latitude 29.591°S and a longitude of 27.452°E. The measurements were taken at a height of 2,014 m above sea level, as shown in Figure 5.

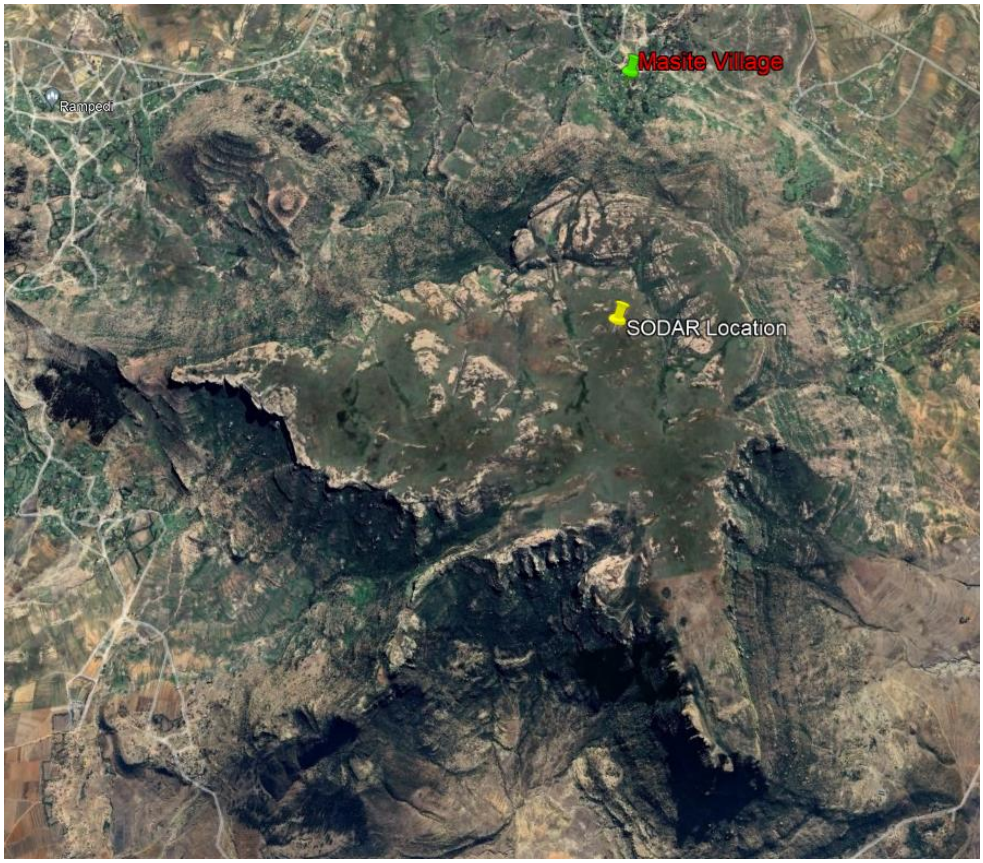

Figure 5: View of Rothe Plateau from Google Earth

3.2. Overview of REMTECH PA-XS SODAR

PA-XS SODAR has a vertical range of 20–300 m above ground level; it records wind speed data every 10 minutes on average. The 10 minutes time interval was averaged into 1 hour intervals for easy comparison with the ERA 5 dataset, which comes in hourly intervals. Hourly datasets have a low resolution when compared to 10-minute datasets, thus introducing errors. SODAR has five beams, one vertically pointed for vertical wind speed measurements and four slanted beams, as seen in Figure 6. These 2 by 2 symmetrical slanted beams are 22.5° from vertical. To prevent sound echoes, an obstacle should not be visible above an elevation of 20° from the surface level. During the measurement period, the solar panel with a rated voltage of 18.6 volts, a rated power of 160 watts and a rechargeable backup battery of 12 volts and 100 AH provided power to the SODAR device. The PA-XS SODAR had a power consumption of 18 watts, which necessitated the use of a solar panel with a capacity of at least 216 watts.

A laptop was used for communicating with the SODAR via Ethernet or Wi-Fi (setting up operating parameters like time, date, downloading data, etc.). Remote retrieval of SODAR data was possible using satellite terminal options or a 4G connection. Based on a six-month survey, the final report included data from 20 m at increments of 50 m up to 270 m, as shown in Table 5. The 50-meter increment indicates that each measurement covered a larger area of the atmosphere. This mitigated the effects of localized turbulence, resulting in more steady and trustworthy data. Larger spacing also produces a smoother picture of the wind profile. This helped to filter out noise and to increase the signal-to-noise ratio, hence boosting data accuracy [75].

Table 5: Basic information of the SODAR measuring tool

Evaluated measurement period	23-01-2024 to 31-07-2024
Remote sensing device model	SODAR PA-XS
Unit serial number	9600
Selected measurement heights	20 m, 70 m, 120 m, 170 m, 220 m, and 270

	m
Beam angle from vertical	22.5^{o}
Power supply	Solar photovoltaic (PV) with battery storage

To compute unprocessed acoustic spectra, REMTECH SODAR employed the fast Fourier transform (FFT). In the receive mode, the reflected signal undergoes initial processing with 2,048 frequency-point FFTs.

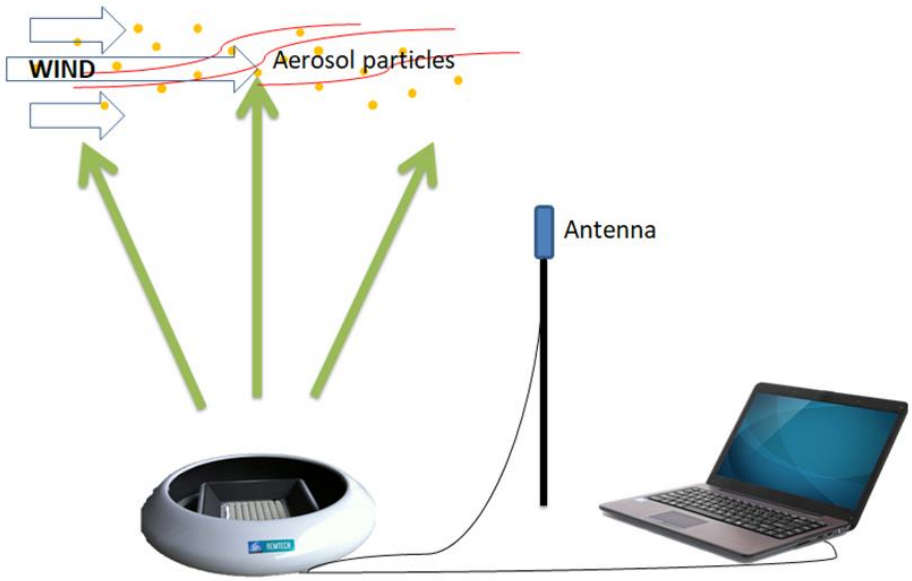

Figure 6: Measuring principle of REMTECH PA-XS SODAR's wind speed and direction

3.3. Data filtering

Horizontal wind speed was measured at elevations above ground level ranging from 20 m to 270 m in increments of 50 m. The SODAR data block presented all mean readings of horizontal wind speed, direction, and vertical wind speed every 10 minutes, as seen in Table 6. The REMTECH PA-XS SODAR monitored the signal-to-noise ratio (SNR) which served as the internal quality control metric used to filter the data, every 10 minutes. All of this was done at regular intervals

when the SODAR was not emitting but still performing all of its routine computations. Furthermore, before any analysis was performed on the SODAR data, it was filtered by eliminating the erroneous and suspect data that was displayed by the value -9999. The wrong peaks in the acoustic spectrum of a backscattered signal, which could be acoustic, electrical, or magnetic, can lead to erroneous and suspicious data, which is what Table 7 shows.

Table 6: SODAR measurement data block

ALT	Line 1, altitude in meters
CT	Echo strength (no units)
SPEED	Horizontal wind speed in cm/s
DIR	The wind direction in degrees
W	Vertical wind speed in cm/s

Table 7: Example of raw SODAR data with errors

Date	Echo (CT)	Speed cm/	Direction	Vertical W	T IN	PmBARS	T out	RH%
23/01/2024 11:20	-9999	-9999	-9999	-9999	29	806	22,7	55,7
23/01/2024 11:30	-9999	-9999	-9999	-9999	35,9	805,8	22,7	54,7
23/01/2024 11:40	93	502	64	-5	40,2	806	22,8	52,7
23/01/2024 11:50	131	672	47	19	42,4	805,8	22,2	53,7
23/01/2024 12:00	131	606	59	52	43,6	805,8	23,6	51,9
23/01/2024 12:10	128	558	74	26	44,4	805,8	24	51,9
23/01/2024 12:20	136	510	75	17	44,9	805,6	23,9	50,2
23/01/2024 12:30	164	540	68	-31	45,3	805,6	23,7	52,2
23/01/2024 12:40	129	604	65	-19	45,6	805,7	23,3	52,9
23/01/2024 12:50	84	535	56	0	45,3	805,5	22,7	54,2
23/01/2024 13:00	52	511	78	39	44,7	805,6	22,7	52,3
23/01/2024 13:10	59	483	78	1	44,2	805,4	23,3	52,9
23/01/2024 13:20	75	499	74	-35	44,1	805,5	23,1	53,4
23/01/2024 13:30	184	543	65	-10	44,2	805,3	24,2	47,7
23/01/2024 13:40	123	458	57	9	44,4	805,3	23,3	48,1
23/01/2024 13:50	92	469	56	-14	44,3	805,1	22,5	51,7
23/01/2024 14:00	95	474	49	-13	44	805,2	22,1	51
23/01/2024 14:10	64	518	46	-5	43,5	805,1	21,5	53,5
23/01/2024 14:20	24	547	47	-12	42,9	805,2	20,9	53,9
23/01/2024 14:30	28	566	42	-24	42,1	804,9	20	60,8
23/01/2024 14:40	32	639	43	-32	41,2	805	19,5	62,5

3.4. Data Analysis using Wind Atlas Analysis and Application Program (WAsP)

WAsP is an industry-standard programme that extrapolates wind data statistics. It was utilized to simulate the effects of impediments, surface roughness and terrain height change as well as to provide observed wind data (wind speed and direction analysis) for the potential farm. This wind data was uploaded to the WAsP Climate Analyst (WACA) to offer an analysis of wind speed distribution for the six months of the measuring campaign. ERA 5 data was also uploaded into WACA for analysis. For each of the uploads, a report was generated; the WACA employed the Weibull distribution function, which offered a profile of wind speed and power density for each wind direction. This WACA data was utilized to generate a file of the observed mean wind climate (OMWC) for the Rothe Plateau; it helped to determine changes in form factors from sector to sector.

3.4.1. Weibull Distribution

The Weibull distribution variables, described in Section 2.5.2, were used to establish the shape (how the probability density is spread out among various values) and scale (influencing the

dispersion of the data surrounding the average wind speed) of the distribution, respectively. The Weibull distribution probability density function (PDF), given by Equation 16, was utilized in WAsP to illustrate the chance of certain wind speeds occurring within a specific range of a measured period. Modeling wind speed data assists in analyzing the frequency of different wind speeds, which in turn aids in assessing the wind power potential.

3.5. Extracting Modeled Wind Speeds using the Numerical Dataset (ERA 5)

The European Centre for Medium-Range Weather Forecasts (ECMWF) implemented wind speed fields downloaded from Copernicus (Europe's Eyes on Earth). For six months, the ERA 5 hourly data on single levels from 1940 to the present reanalysis dataset in the format NetCDF (experimental) was downloaded at 100 meters *u* and *v* wind components. The *u* component shows the direction of the wind from east to west and the *v* component shows the direction of the wind from north to south. The wind speed was calculated using Equation 22 from the *u* and *v* components of the wind illustrated in Figure 7. Wind direction increases clockwise; therefore, a northerly wind is zero degrees; an easterly wind is 90 degrees; a southerly wind is 180 degrees and a westerly wind is 270 degrees.

$$WS = \sqrt{u^2 + v^2} \qquad \text{Equation 22}$$

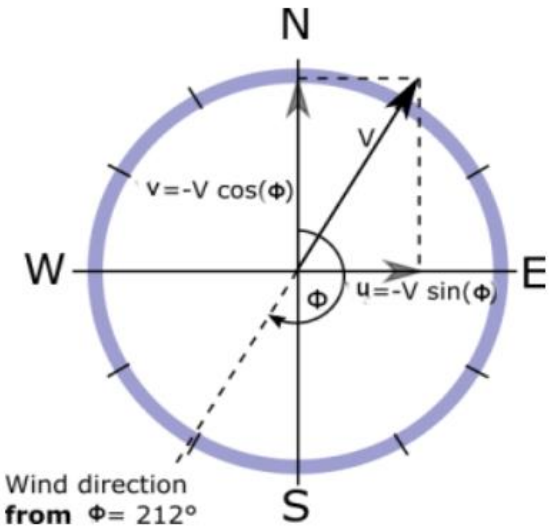

Figure 7: The meteorological wind direction from which the wind blows [76].

Wind direction (WD) was calculated using Equation 23, giving WD in degrees in the range $0 \leq \emptyset < 360$.

$$WD(\emptyset) = MOD\left(180 + \frac{180}{\pi} ATAN2(u, v), 360\right) \quad \text{Equation 23}$$

To narrow the sub-region on which the data was extracted, the north, west, south, and east were clipped at -29.58 degrees, 27.45 degrees, -29.59 degrees, and 27.44 degrees, respectively. The selection of these coordinates was deliberate to concentrate on a particular geographical point where the SODAR was located, guaranteeing that the analysis is relevant to the site where wind data are being compared and validated, which is at longitude 27.45^0 and latitude -29.59^0. The single coordinate representation is displayed in one of the corners of the rectangle bounding box illustrated in Figure 8. A coordinate denotes a distinct location inside the dataset grid.

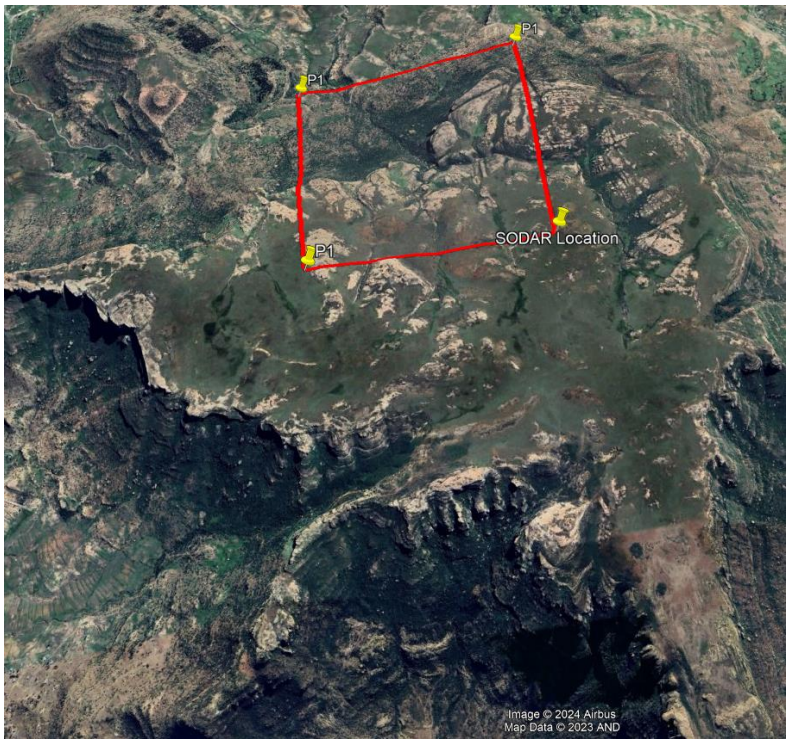

Figure 8: Sub-region rectangular bounding box

3.6. Extrapolation of wind speed

To make it possible to compare the ERA 5 data that was downloaded at a height of 100 m with the SODAR data that was taken at 120 m, the data that was downloaded at a height of 100 m was

extrapolated to 120 m using the logarithmic law displayed by Equation 17. Unlike the power law, the logarithmic law does not necessitate the shear exponent but relies on the surface roughness length, which can be approximated depending on the terrain. The roughness height Z_0 was assumed to be 0.03 m because of minimal obstacles close to the measuring site. This extrapolation ensured the comparison of the wind speeds at 120 meters between the two datasets.

Wind shear was described in Equation 24 as a shift in wind speed over a particular vertical distance. The terrain, atmospheric turbulence, and surface roughness can all affect wind shear [58].

$$\alpha = \frac{ln\left(\frac{V(Z)}{V(V_R)}\right)}{ln\left(\frac{Z}{Z_0}\right)} \qquad \text{Equation 24}$$

Frictional forces, large structures, trees, shrubs, forests, and irregularities affect wind flow. As a result, such elements have an enormous effect on the overall roughness of the surrounding landscape.

3.7. Validating Reanalysis Dataset (ERA 5)

Validation assesses how well a model replicates the real world for a certain application. It was performed after removing erroneous and suspicious data to guarantee that the validation process uncovers model flaws. The assumption was made that the SODAR measurements are accurate with only minor inaccuracies. The reason for this is that SODAR measurements are acquired directly from the specific location of interest, offering localized and site-specific data that accurately reflects the immediate atmospheric conditions [59]. To find out how REMTECH PA-XS SODAR data fared compared to the ERA 5 data, statistical tools such as the correlation coefficient *R*, the mean bias error (MBE), the normalized root mean square error (NRMSE) and the standard deviation were used. The correlation coefficient measures the degree of linear correlation between ERA 5 and REMTECH PA-XS SODAR data. To obtain positive linear correlations ranging from 0 to 1, the determination coefficient R^2 demonstrated by Equation 8 was used. The ERA 5 model was selected for comparison since Hirundo Energy utilized it in their wind farm feasibility assessment, which was for a period of 30 years (1989-2018). The dataset of this model offers a comprehensive view on atmospheric conditions over an extended period.

3.8. Design of the Wind Farm

WAsP and Google Earth Pro are the two software programmes that were utilized in the design of the wind farm located on the Rothe Plateau. In the WAsP software, the average temperature from SODAR data and the height from which the measurements were taken above sea level were used to calculate air density. Equation 15 was employed to manually compute the air density using temperature and pressure. This determined air density was then compared with the air density calculated in WAsP to generate a prediction for the Rothe Plateau. Based on the anticipated wind conditions, a wind farm was constructed. The placement of the turbines and the various terrain heights were all visualized using Google Earth Pro.

The OMWC file, derived by the WAsP climate analyzer (WACA), was imported into WAsP using the converted UTM coordinates 539826 for the X coordinate and 6723624 for the Y coordinate. To observe the topography surrounding the wind measurement location, a vector map of the location was also added. The turbine generator that was chosen for this case study was the Vestas V162-6.0 MW, according to the developer's recommendation (Hirundo Energy). It has a maximum rated power output of 6.0 MW and a rotor diameter of 162 m.

Equation 20 was used to calculate the turbulence intensity, which has a direct impact on the effectiveness, performance and the structural integrity of wind turbines. High turbulence intensity can result in heightened mechanical strain and fatigue on turbine parts, thus diminishing the turbine lifespan and escalating the maintenance expenses. The variability and inconsistency of wind speed have an impact on the capacity to estimate and maintain a steady power output accurately. This can create challenges when integrating wind energy into the power grid and planning for energy needs. Furthermore, turbulence has an impact on the wake effect, leading to a decrease in the effectiveness of turbines located downstream in a wind farm.

The capacity factor was then computed by dividing the annual energy production that was computed in WAsP by the maximum power output that would have been produced if every turbine had been operating at full capacity for 8,760 hours (1 year), as demonstrated by Equation 21.

4. RESULTS AND DISCUSSION

4.1. Overview

The SODAR and ERA 5 raw data were analyzed using the Wind Atlas Analysis and Application Program (WAsP). The study examined the primary findings derived from the raw SODAR and ERA 5 data, focusing on wind speed distribution, estimations of turbulence strength, and wind shear. It also looks at what these results mean for wind energy applications and whether or not wind power can be adequately generated at the site. This chapter also shows the designed wind farm on the Rothe Plateau, at a hub height of 120 m. However, the main purpose of this project is to validate the ERA 5 data against the SODAR data.

4.2. Observed Mean Wind Climate (OMWC) for SODAR and ERA 5 Data

The data acquired from the SODAR device was from the day of installation, 23 January 2024, to 31 July 2024. Despite the difficulty in obtaining data due to the inadequate power supply, the SODAR system offered insights into the wind profile while it was in service. After filtering to eliminate any data that would jeopardize the accuracy of the wind estimate, 2,623 acceptable data readings were used, representing 57.36% of the 4,573 intended recording count, as shown in Table 8. The availability of obtained and processed data for quality SODAR is above 90% [45]. The wind speed data range that was considered acceptable ranged from 1.70 m/s to 19.41 m/s.

Due to battery limitations, the system was only able to operate during the day but not on cloudy days, which introduced a bias in the dataset because nocturnal wind patterns, which frequently diverge greatly from daytime patterns, were underrepresented. This has an impact on the representation of the wind regime at the site, which is necessary for validation purposes and to forecast the energy yields of the wind farm.

The ERA 5 reanalysis data was refined to have the equivalent SODAR time series to guarantee that the datasets encompass identical periods, enabling a fair and reliable comparison. The acceptable range for ERA 5 wind speed data was from 0.08 m/s to 12.38 m/s.

Table 8: WAsP Climate Analyst-generated imported wind data report (a) SODAR and (b) ERA 5.

Recordings in file	
Recordings in file:	2623
Missing records:	1950
Recording interval (s) :	3600
Start time:	2024-01-23T11:00:00
End time:	2024-07-31T23:00:00
Mean wind speed data:	
Data column no. in source file :	4
Discretisation width :	0.01
Multiplier :	1
Offset :	0
Averaging time (s) :	3600
Lower limit :	0.00
Readings below lower limit :	None
Upper limit :	90.00
Readings above upper limit :	None
Calm threshold :	0.00 m/s
Count of calms :	1 (0.04 %)
Valid readings accepted:	2623 (100.00 %)
Accepted values range:	1.70m/s to 19.41m/s
Mean wind direction data:	
Data column no. in source file :	5
Discretisation width :	0.01
Multiplier :	1
Offset :	0
Averaging time (s) :	3600
Lower limit :	0.00
Readings below lower limit :	None
Upper limit :	360.00
Readings above upper limit :	None
Calm threshold :	0.00 m/s
Count of calms :	None
Valid readings accepted:	2623 (100.00 %)
Accepted values range:	9.00° to 351.80°
Data recovery:	
Expected recording count:	4573
Count of recordings in file:	2623 (57.36 %)
Recordings with invalid values in one or more fields:	0 (0.00 %)
Entirely valid recordings accepted:	2623 (57.36 %)
Recovery percentage (vs. expected):	57.36 %

(a)

Recordings in file	
Recordings in file:	2623
Missing records:	1950
Recording interval (s) :	3600
Start time:	2024-01-23T11:00:00
End time:	2024-07-31T23:00:00
Mean wind speed data:	
Data column no. in source file :	5
Discretisation width :	0.001
Multiplier :	1
Offset :	0
Averaging time (s) :	3600
Lower limit :	0.00
Readings below lower limit :	None
Upper limit :	90.00
Readings above upper limit :	None
Calm threshold :	0.00 m/s
Count of calms :	1 (0.04 %)
Valid readings accepted:	2623 (100.00 %)
Accepted values range:	0.08m/s to 12.38m/s
Mean wind direction data:	
Data column no. in source file :	6
Discretisation width :	0.001
Multiplier :	1
Offset :	0
Averaging time (s) :	3600
Lower limit :	0.00
Readings below lower limit :	None
Upper limit :	360.00
Readings above upper limit :	None
Calm threshold :	0.00 m/s
Count of calms :	None
Valid readings accepted:	2623 (100.00 %)
Accepted values range:	0.79° to 359.75°
Data recovery:	
Expected recording count:	4573
Count of recordings in file:	2623 (57.36 %)
Recordings with invalid values in one or more fields:	0 (0.00 %)
Entirely valid recordings accepted:	2623 (57.36 %)
Recovery percentage (vs. expected):	57.36 %

(b)

Figure 9 depicts the valid time series wind speed (m/s) and direction (∘), the data generated from the SODAR and ERA 5 imported data in the WAsP Climate Analyst. Data gaps during overcast periods indicate a persistent pattern of missing data. The wind offers a visual overview of the frequencies of wind direction, displaying the dispersion of wind patterns, thus providing information on the frequency of wind coming from various directions throughout a specific time frame.

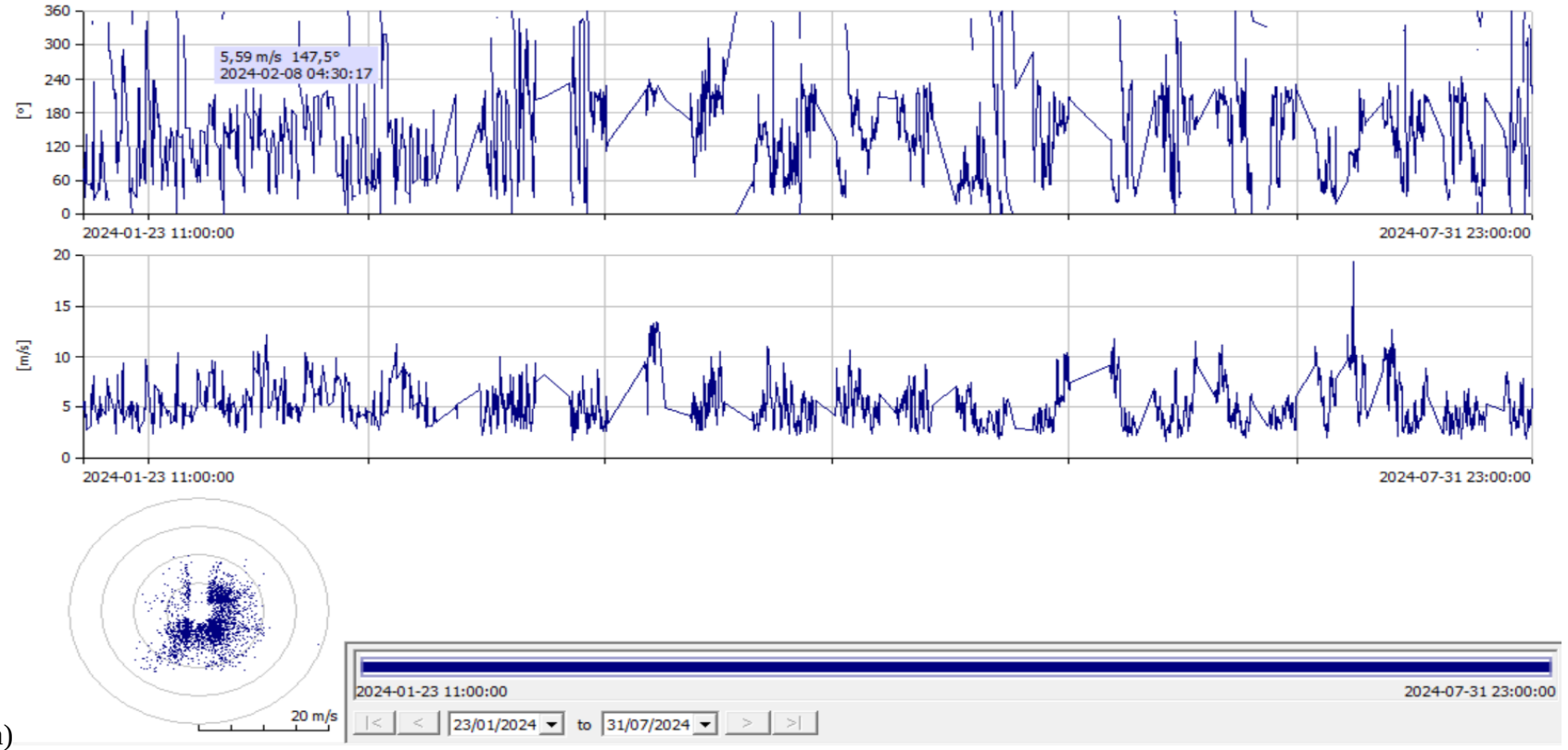

(a)

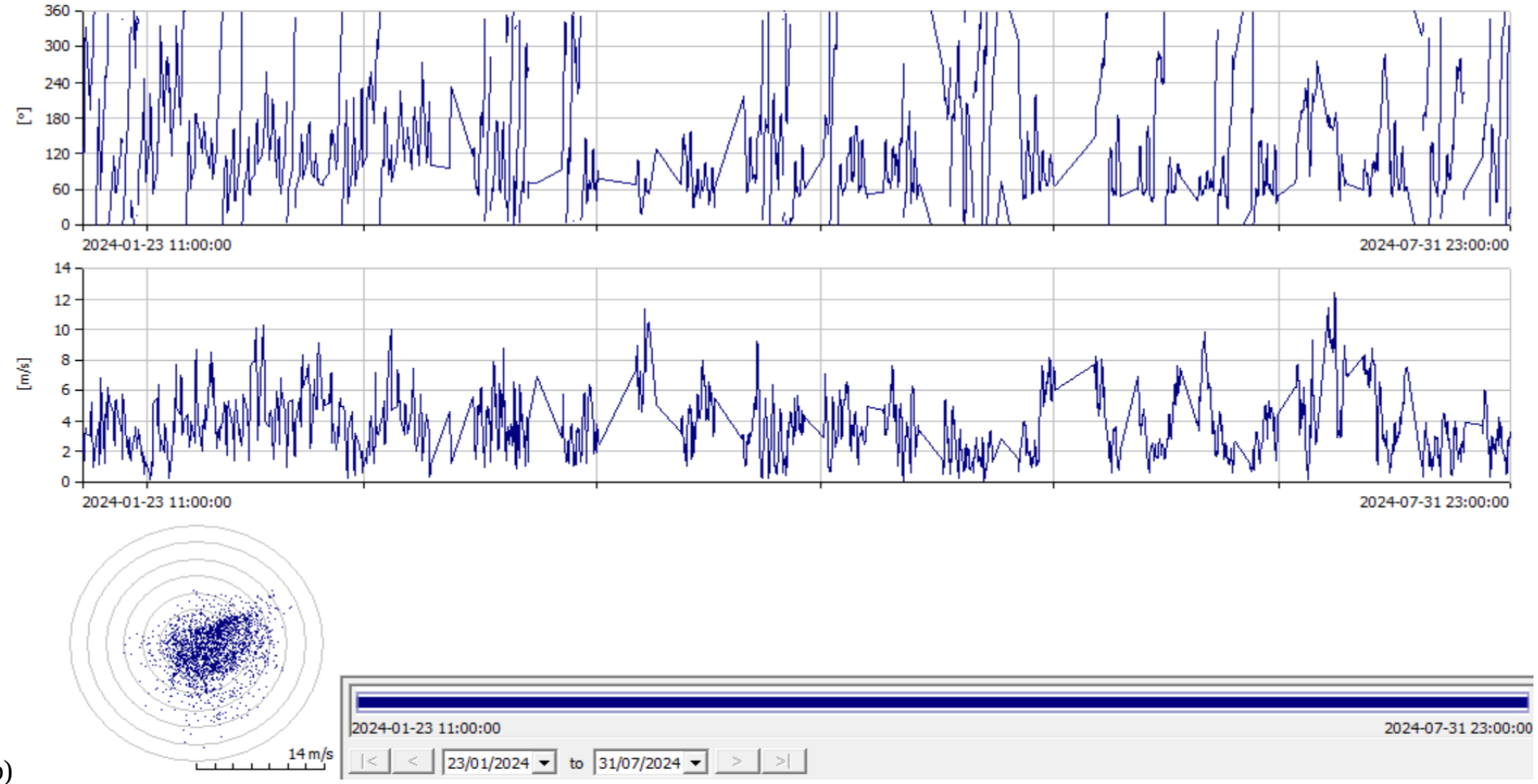

(b)

Figure 9: Validity of the accepted imported data (a) SODAR and (b) ERA 5.

Figure 10 displays the wind rose, indicating that the majority of the wind originated from the south-southeast (SSE) direction at 150° for SODAR. It is important to optimize the configuration and positioning of wind turbines to maximize the collection of wind that gives the most energy. In addition, it demonstrates that the SODAR device's overall average wind speed at 120 m above ground level is 5.1 m/s. A Weibull distribution shape parameter (*k*) was determined to be 2.09. As *k* increases, the wind speeds are getting closer to the mean value. The Weibull distribution scale factor (*c*) was found to be 5.7 m/s.

For ERA 5, the majority of the wind blew from a direction of 60°, east-northeast (ENE). For all the sectors, an average wind speed is 3.8 m/s at 120 m above ground level, with a shape factor *k* of 1.81 indicating a fairly variable wind profile and a scale factor *c* of 4.2 m/s.

(a)

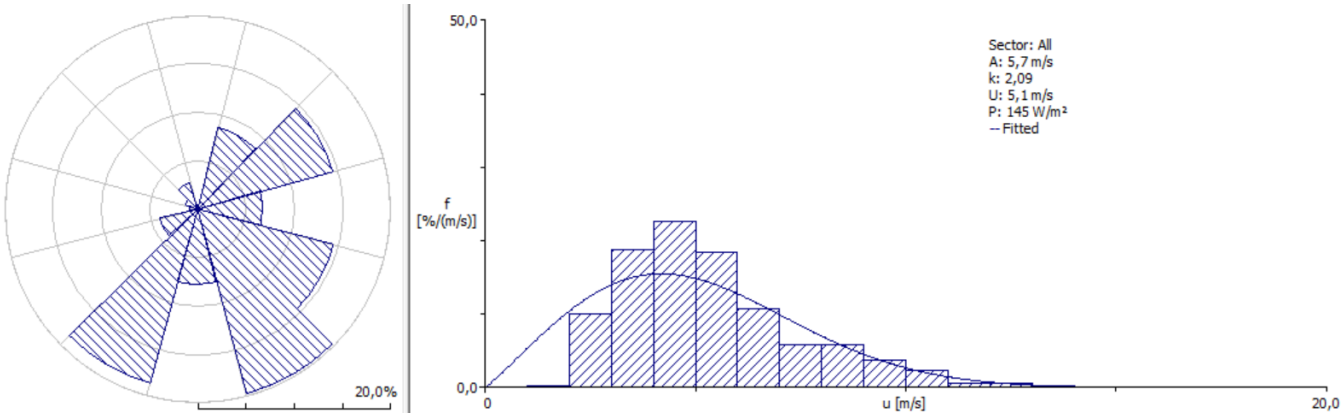

(b)

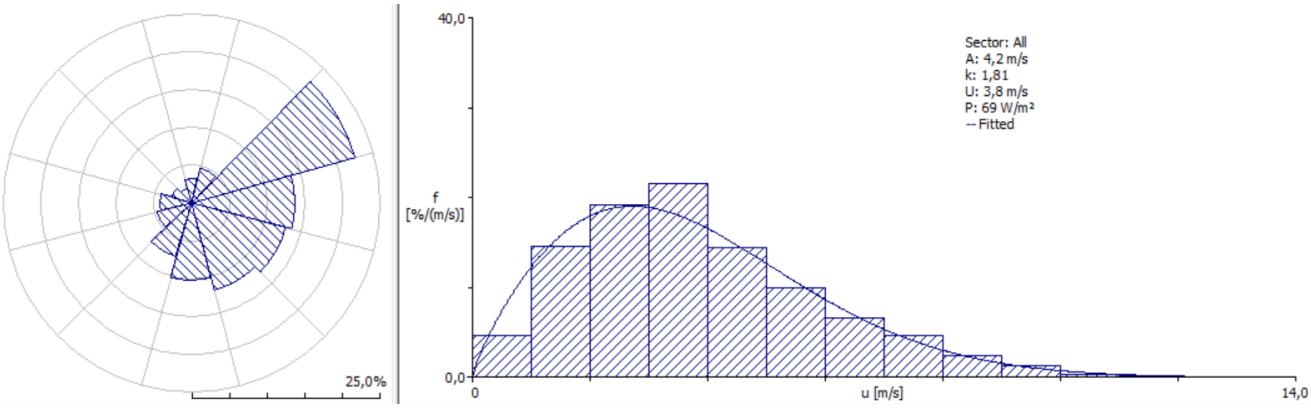

Figure 10: Wind rose of the observed mean wind climate with Weibull distribution for all sectors (a) SODAR (b) ERA 5.

4.2.1. Wind Speeds Variation by Hours and Months

Table 9 demonstrates an analysis of wind speed patterns across various time periods, illustrating the fluctuations in average wind speed for each hour and month between January and July. For ERA 5, the data was collected at a height of 100 meters above ground level (a.g.l) and extrapolated at a height of 120 meters a.g.l. Both SODAR and ERA 5 show that most of the time, between ten o'clock in the morning and three o'clock in the afternoon, the wind speeds are typically at their highest. This is because under normal conditions, the ground is probably at its hottest, and the air is most actively mixed as a result of hot air that is rising and cold air that is descending. During the night, wind speeds often drop as the atmosphere becomes more stable, resulting in reduced turbulence and a decrease in wind speeds [77].

Table 9: Mean wind speed variations by hours and months (a) SODAR (b) ERA 5.

(a)

All-sectors statistics

	Weibull-A	Weibull-k	Mean speed	Power density
Source data (2623)	-	-	5,36 m/s	144 W/m²
Fitted	5,7 m/s	2,09	5,06 m/s	145 W/m²
Emergent	-	-	5,06 m/s	145 W/m²
Combined	5,7 m/s	2,10	5,06 m/s	145 W/m²

Mean wind speeds (hourly, by month)

Hour	Jan	Feb	Mar	Apr	May	Jun	Jul	Aug	Sep	Oct	Nov	Dec	Year
0	---	---	5.29	5.29	4.66	5.58	5.09	---	---	---	---	---	5.18
1	---	---	5.13	5.72	4.79	5.39	5.01	---	---	---	---	---	5.21
2	---	---	4.99	5.71	5.15	5.42	5.01	---	---	---	---	---	5.26
3	---	---	5.27	5.19	4.96	5.17	4.64	---	---	---	---	---	5.05
4	---	---	5.55	4.94	4.93	4.83	4.54	---	---	---	---	---	4.96
5	---	---	5.46	5.07	4.74	4.82	4.49	---	---	---	---	---	4.92
6	---	---	5.43	5.21	4.45	4.28	4.40	---	---	---	---	---	4.75
7	---	6.41	5.29	5.60	4.27	4.32	5.05	---	---	---	---	---	5.16
8	---	5.88	5.41	5.44	4.39	4.50	5.05	---	---	---	---	---	5.11
9	3.97	5.83	4.98	5.60	4.74	4.70	6.10	---	---	---	---	---	5.13
10	4.44	5.90	4.59	5.91	5.26	4.88	5.74	---	---	---	---	---	5.25
11	4.94	6.03	4.93	5.83	5.77	5.10	6.37	---	---	---	---	---	5.57
12	5.16	6.09	5.43	5.85	6.05	5.53	6.51	---	---	---	---	---	5.80
13	5.10	5.87	5.90	6.09	5.71	5.25	6.36	---	---	---	---	---	5.75
14	5.44	5.49	5.66	5.96	5.38	5.03	6.47	---	---	---	---	---	5.63
15	6.03	5.62	5.70	5.69	4.80	4.81	5.74	---	---	---	---	---	5.48
16	5.58	5.61	5.48	5.24	4.99	5.06	5.84	---	---	---	---	---	5.40
17	4.75	5.61	5.18	5.51	5.05	4.88	6.16	---	---	---	---	---	5.31
18	4.96	5.75	5.42	6.04	5.47	5.06	6.33	---	---	---	---	---	5.57
19	4.84	5.93	5.14	5.66	5.03	5.22	6.24	---	---	---	---	---	5.44
20	5.27	5.74	4.64	5.83	5.06	5.13	5.92	---	---	---	---	---	5.37
21	5.72	5.88	4.14	6.30	5.02	5.28	5.62	---	---	---	---	---	5.42
22	---	---	4.68	5.78	4.85	5.45	5.50	---	---	---	---	---	5.25
23	---	---	4.35	6.55	4.93	5.34	5.50	---	---	---	---	---	5.33
Average	5.09	5.84	5.17	5.67	5.02	5.04	5.57	---	---	---	---	---	5.30

Mean wind speeds (yearly, by month)

Year	Jan	Feb	Mar	Apr	May	Jun	Jul	Aug	Sep	Oct	Nov	Dec	Year
2024	5.10	5.80	5.20	5.66	5.03	5.04	5.60	---	---	---	---	---	5.35

(b)

All-sectors statistics

	Weibull-A	Weibull-k	Mean speed	Power density
Source data (2623)	-	-	3,84 m/s	69 W/m²
Fitted	4,2 m/s	1,81	3,77 m/s	69 W/m²
Emergent	-	-	3,77 m/s	69 W/m²
Combined	4,2 m/s	1,82	3,77 m/s	70 W/m²

Mean wind speeds (hourly, by month)

Hour	Jan	Feb	Mar	Apr	May	Jun	Jul	Aug	Sep	Oct	Nov	Dec	Year
0	---	---	3.776	3.124	2.812	4.236	3.814	---	---	---	---	---	3.552
1	---	---	3.883	3.114	3.011	4.260	3.917	---	---	---	---	---	3.637
2	---	---	4.026	3.408	3.310	4.332	3.752	---	---	---	---	---	3.766
3	---	---	3.987	3.436	3.217	4.165	3.549	---	---	---	---	---	3.671
4	---	---	3.932	3.650	3.304	4.065	3.290	---	---	---	---	---	3.648
5	---	---	3.989	3.821	3.090	4.338	3.351	---	---	---	---	---	3.718
6	---	---	3.543	3.759	3.121	3.995	3.450	---	---	---	---	---	3.573
7	---	5.052	3.671	3.722	3.013	3.899	3.453	---	---	---	---	---	3.802
8	---	4.600	4.008	4.246	2.900	3.395	3.283	---	---	---	---	---	3.739
9	2.680	4.561	4.201	5.103	3.425	3.559	3.875	---	---	---	---	---	3.915
10	2.868	4.455	4.302	5.501	4.024	3.728	4.032	---	---	---	---	---	4.130
11	2.992	4.454	4.490	5.473	4.308	3.676	4.282	---	---	---	---	---	4.239
12	3.422	4.528	4.820	5.325	4.390	3.740	4.914	---	---	---	---	---	4.448
13	3.540	4.580	4.999	4.983	4.279	3.451	4.609	---	---	---	---	---	4.349
14	3.279	4.503	4.642	4.613	3.962	3.150	4.689	---	---	---	---	---	4.120
15	3.075	4.029	4.003	4.172	3.560	3.223	4.234	---	---	---	---	---	3.757
16	2.275	3.495	3.535	4.010	3.585	3.511	4.460	---	---	---	---	---	3.553
17	2.593	3.553	3.422	4.014	3.182	3.521	4.636	---	---	---	---	---	3.560
18	3.117	3.983	3.285	4.148	3.289	3.723	4.496	---	---	---	---	---	3.720
19	3.650	4.482	3.169	3.969	3.025	3.890	4.231	---	---	---	---	---	3.774
20	4.134	4.511	2.844	3.932	2.825	3.694	4.170	---	---	---	---	---	3.730
21	3.996	4.533	2.334	3.661	2.632	3.673	4.012	---	---	---	---	---	3.549
22	---	---	2.547	2.930	2.629	3.757	3.887	---	---	---	---	---	3.150
23	---	---	2.949	3.513	2.736	3.861	3.919	---	---	---	---	---	3.396
Average	3.202	4.354	3.765	4.068	3.318	3.785	4.013	---	---	---	---	---	3.771

Mean wind speeds (yearly, by month)

Year	Jan	Feb	Mar	Apr	May	Jun	Jul	Aug	Sep	Oct	Nov	Dec	Year
2024	3.172	4.305	3.849	4.102	3.338	3.766	4.028	---	---	---	---	---	3.794

4.4. Comparison of Remtech PA-XS SODAR with ERA 5 Data

Remtech PA-XS SODAR and ERA 5 both provide useful sources of atmospheric data; however, they diverge in numerous important ways. The major difference between SODAR and ERA 5 is the spatial coverage and resolution of the data. SODAR observations are limited to a single point or a small area, yielding high-resolution vertical profiles but with limited spatial coverage. ERA 5 covers practically the whole world with a rather coarse spatial resolution, making it suitable for large-scale analysis but less detailed for local-scale study. SODAR offers data with a high level of temporal resolution, averaging every 10 minutes. This allows for detecting small-scale changes in wind speed and direction, which are important for a time-sensitive analysis such as evaluating wind shear and turbulence. On the other hand, ERA 5 provides data with hourly intervals, giving a wider view of time and covering a large area. Thus, the assumption was made that SODAR data is accurate compared to ERA 5.

To compare the two, the 10-minute data from the SODAR is synchronized with the hourly data from ERA 5 by averaging the SODAR data to match the hourly intervals. Statistical measures are employed to measure agreement and to detect systematic discrepancies.

4.5. Statistical Analysis of the Remtech PA-XS SODAR and ERA 5 Data.

The validation of SODAR observations and ERA 5 data relies on the correlation coefficient (R), the standard deviation, the coefficient of determination (R^2), the mean biased error (MBE) and the normalized root mean square error (NRMSE), as they are effective in offering a comprehensive statistical analysis of wind data. These methods are employed in the validation of wind data because they have the capability to encompass several areas of data comparison.

The correlation coefficient (R) quantifies the degree of the linear association between SODAR and ERA 5, indicating the extent to which they conform to a common trend. The standard deviation of the disparities between the SODAR and ERA 5 datasets quantifies how much they diverge from one another. The coefficient of determination (R^2) measures the extent to which one dataset explains the variation in another dataset, serving as an indicator of the quality of the fit. The mean biased error (MBE) quantifies the systematic biases by calculating the average difference between SODAR and ERA 5 data. The NRMSE is a statistical measure that standardizes the RMSE, enabling the comparison of errors concerning the average value of the observed data. Employing these techniques in conjunction guarantees a strong and comprehensive evaluation, thus emphasizing the precision and reliability of the datasets and eventually improving the confidence of wind resource assessments.

Finding the correlation value showed how closely the ERA 5 and SODAR wind speeds were similar. A high correlation coefficient, close to 1, means that the two sets of data are very similar. This shows that the SODAR readings fit the ERA 5 data very well. Figure 11 shows the comparison of wind speed measurements obtained from SODAR and ERA 5. Their similarity was measured using the correlation coefficient, Equation 7, which was determined to be 0.725 (72.5%). A correlation coefficient of 72.5% is considered to be relatively strong, suggesting a generally dependable association between the two datasets. However, it also indicates the potential for inconsistencies that may occur from multiple sources, such as variances in the geographical and a temporal resolution of the measurements. These inconsistencies have also resulted in a wind direction correlation coefficient of 27.7%, indicating a relatively poor

correlation. It is normal for the wind speed to correlate well while the wind direction does not [43].

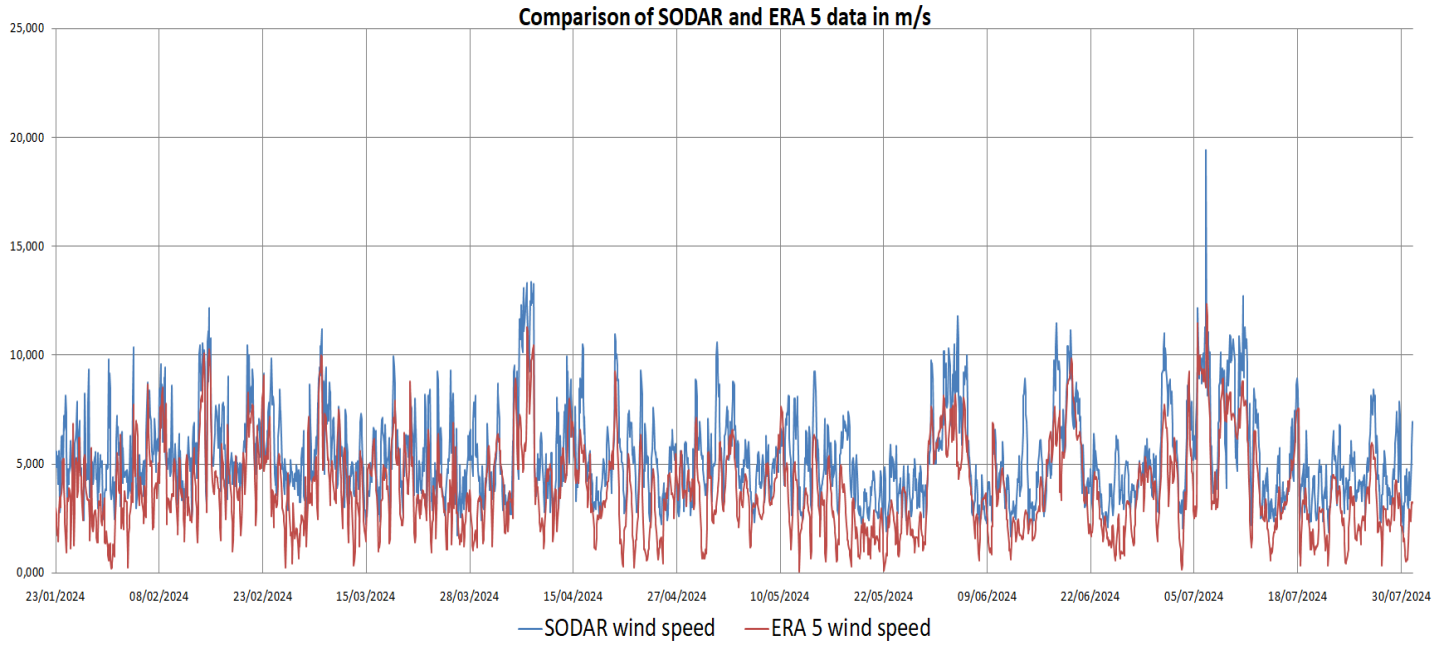

Figure 11: Correlation of SODAR and ERA 5 wind speed data.

Figure 12 shows a coefficient of determination (R^2) of 0.525, which indicates that ERA 5 moderately captures the dynamics that influence the variations in wind speed. However, it may not completely encompass these dynamics. This discrepancy may arise from the ERA 5 inadequate integration of the complex geological characteristics of the Rothe Plateau, which can impact the accuracy of wind speed observations.

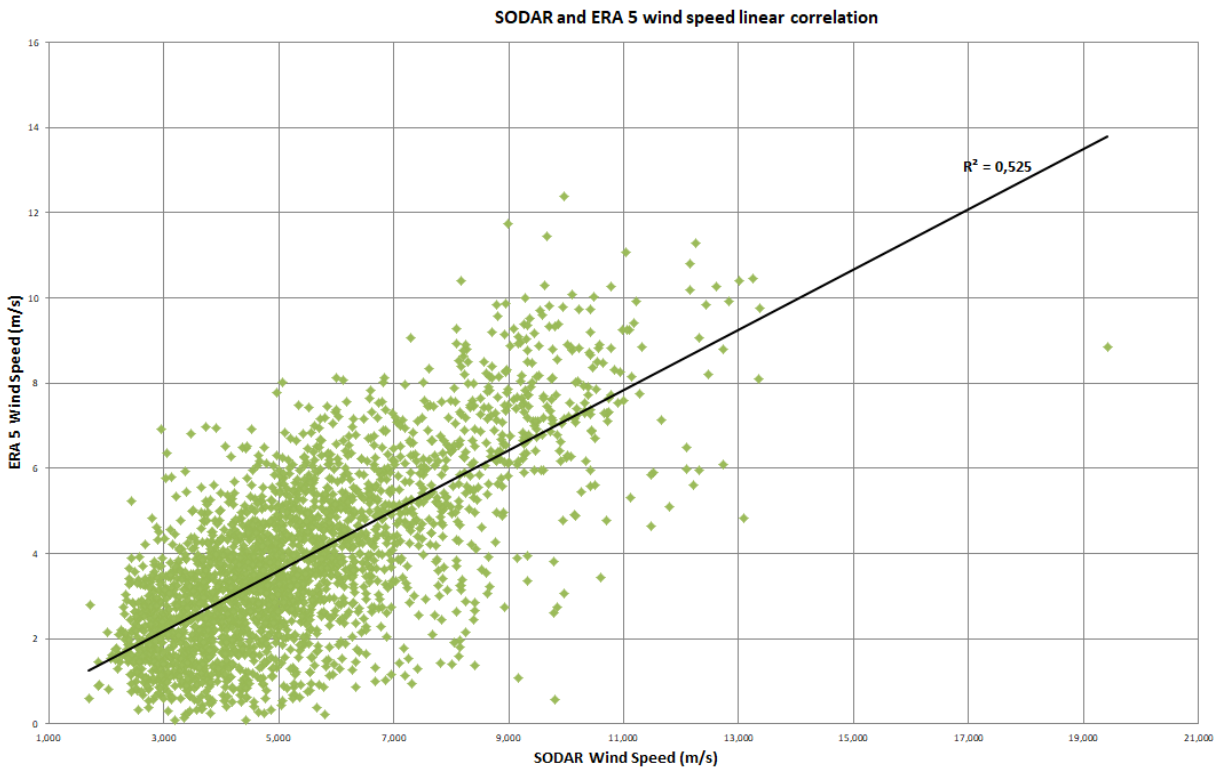

Figure 12: Linear correlation between SODAR and ERA 5.

The mean bias error (MBE) analysis assists in identifying systematic errors in wind speed data that enhances the accuracy of wind resource evaluations. The MBE quantifies the mean difference between wind speeds from ERA 5 and SODAR. It was found to be -1.51 m/s, thus indicating the underestimation of the wind resource at Rothe Plateau by the ERA 5. The MBE for wind direction was also underestimated by -7.84^0. Through the analysis of the MBE, it is easier to identify and to address systematic bias in the data, resulting in more accurate and dependable assessments of wind resources.

The standard deviation of the differences between the two datasets was found to be 1.549 m/s and 122.7^0 for wind speed and direction, respectively. This shows how wind speeds and directions vary concerning the mean, thus showing a considerable degree of variability in wind observations considering the SODAR mean wind speed is 5.1 m/s and the mean direction is 136.0^0. A lower standard deviation in the wind speed data would indicate less variability and higher dependability.

The normalized root mean square error (NRMSE) offers an evaluation of the dataset precision when ERA 5 and SODAR data are compared. By calculating the degree of agreement between the wind speeds obtained from ERA 5 and those recorded by SODAR, NRMSE can help to validate wind data. A smaller NRMSE value suggests a closer match between the two datasets. A NRMSE value of 0.122 was found, showing that the prediction errors are approximately 12.2% of the range of the SODAR wind speed data. This points to a moderate degree of reliability and precision in the ERA 5 data [78]. For wind direction, the NRMSE was found to be 35.9%, which indicates that ERA 5 is providing an inaccurate forecast of wind direction.

4.6. Comparison of Wind Farm Design using SODAR and ERA 5 data

The wind farm design incorporated the utilization of SODAR data to evaluate the wind conditions at a hub height of 120 m. This study examines the influence of topography and surface roughness on accurately mapping the available wind energy potential. The wind farm results were generated using WAsP software on the Rothe Plateau. A 10-meter resolution resource grid was utilized to acquire accurate and dependable results, offering a high level of detail at a small spatial scale.

A wind farm consisting of eight Vestas V162-6.0 MW turbines, each with a hub height of 120 m capable of generating a maximum power output of 6.0 MW was proposed. Given the absence of significant obstacles near the SODAR device, a roughness class of 0.03 m was considered. Figure 13 shows the power curve of the chosen turbine with cut-in speed of 3 m/s and cut-out speed of 24 m/s.

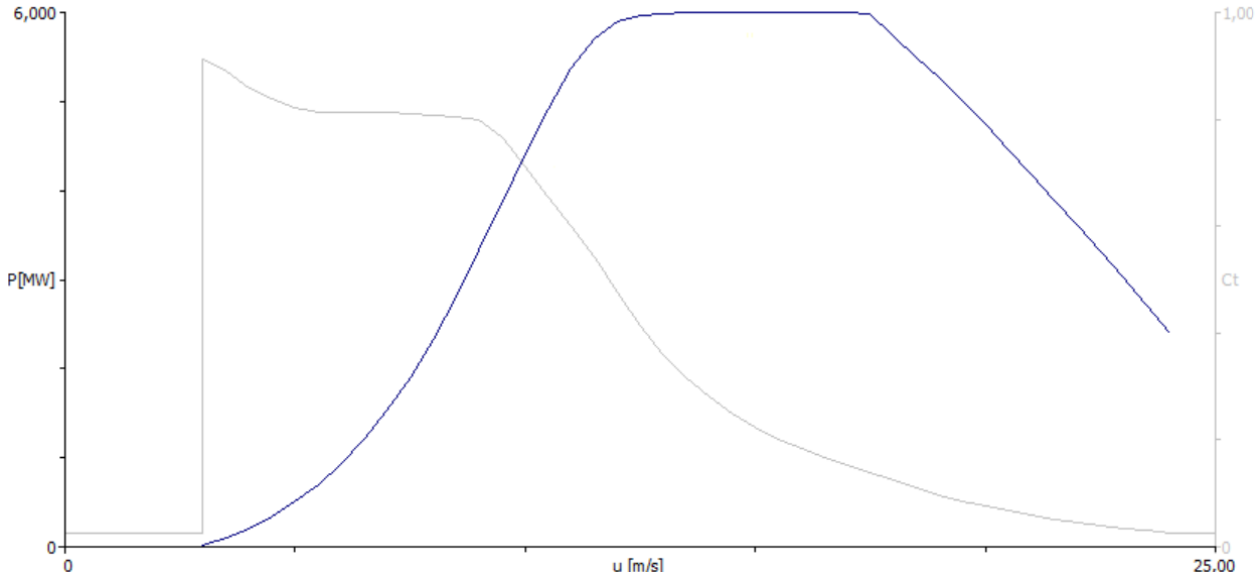

Figure 13: Power curve of a Vestas V162-6.0 MW wind turbine generator.

After extrapolating the ERA 5 data from 100 m to 120 m, the power law in Equation 19 was used to get the wind shear exponent, which was found to be 0.122. The filtered data obtained through the use of the SODAR device was compared to the raw data from ERA 5 to determine energy production. The raw ERA 5 data, initially measured at an elevation of 100 m, was employed for analysis at 120 m to match the desired measurement height.

4.6.1. Wind Speed

On the Rothe Plateau, each turbine wind rose and annual energy production (AEP) is displayed in Figure 14 of the wind speed resource grid. The wind speeds recorded by ERA 5 are lower compared to those obtained using SODAR, probably due to the coarse spatial resolution of ERA 5. This resolution involves averaging wind speeds over the vast grid cells. This results in the smoothing out of local variances. On the other hand, SODAR technology provides precise measurements of wind speeds at the location with a high level of detail in terms of time, allowing for a more accurate representation of local wind patterns. ERA 5 data, which is usually given every hour, may not capture short-term fluctuations and maximum wind speeds. In contrast, SODAR can offer continuous measurements, allowing for the detection of quick changes and gusts.

The reddish areas on the map represent the compressed wind streamlines located toward the top of the hill. These streamlines are responsible for increasing the wind speed. Priority should be given to regions with higher wind speeds to maximize energy capture. The WAsP software generates a spatial distribution with turbine site wind speeds at 120 m hub height ranging from an average of 4.98 m/s to 5.60 m/s for SODAR and 3.79 m/s to 4.63 m/s for ERA 5, as can be seen in Table 12.

(a) 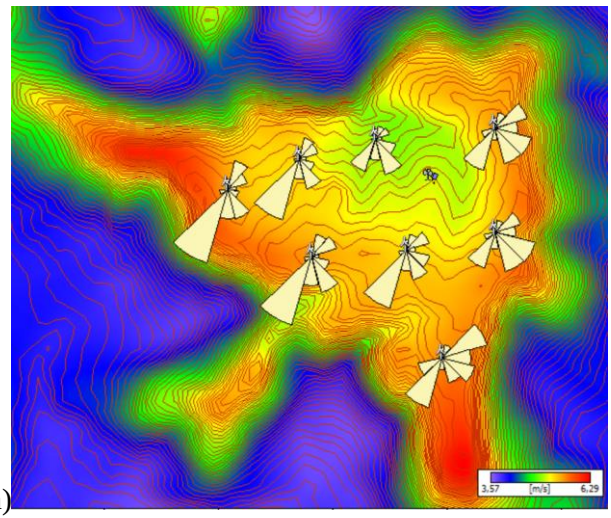 (b) 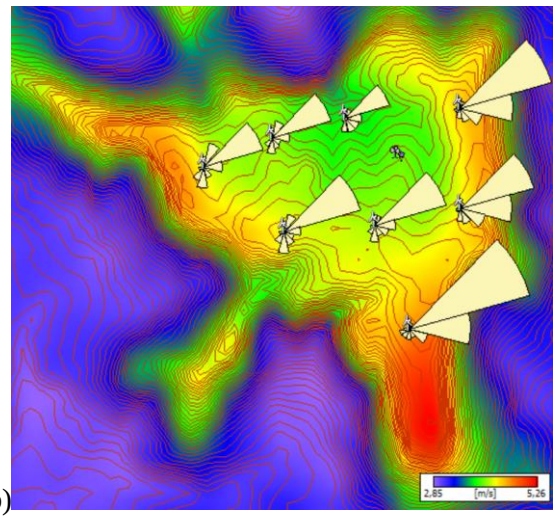

Figure 14: Resource grid displaying the site wind speed and wind rose of the AEP gross and the wake losses (a) SODAR (b) ERA 5.

4.6.2. Air Density

The air density has an impact on the power density of the wind turbines on the Rothe Plateau, which in turn has an impact on the wind farm energy production. Therefore, the air density of the area was determined using the elevation (m) of the SODAR point of measurement capture above sea level and the mean temperature (K). The WAsP software determined that the air density value was 0.95 kg/m^3. By calculating air density using Equation 15, the air density was found to be 0.969 kg/m^3, where the mean temperature was 15.97^{0}C (289.12 K) and the pressure was 803.53 mbar (80353 Pa). This method is employed to account for variations in temperature and pressure across the site. WAsP ensures that these variations are regularly taken into account by employing a standardized procedure. It was developed to utilize computed values to provide precise and dependable evaluations of wind resources; thus, the air density was taken to be 0.95 kg/m^3 [79].

4.6.3. Turbulence Intensity

Turbulence intensity quantifies the variation in wind speed relative to its average value. Furthermore, the turbulence intensity for SODAR was calculated to be 0.394 (39.4%) using Equation 20, which indicates a high level of change in wind speed. This can be attributed to the scarcity of wind data. For ERA 5, the turbulence intensity was calculated to be 55.0%. The standard deviation (σ) of wind speed was calculated. This is because the ERA 5 dataset spatial resolution may not accurately represent small-scale turbulence effects.

4.6.4. Power Density

Figure 15 illustrates the power density resource grid and the variety of power densities in the area for the wind turbines on the Rothe Plateau. The grid shows significant changes based on wind speed and height. The blueish color indicates areas with the least power density and the reddish color indicates areas with the most power density. Higher elevations result in higher power densities due to the observed rise in wind speed with height.

The turbines are located in areas where the power density ranges from 109 W/m^2 to 155 W/m^2 for SODAR and 56 W/m^2 to 109 W/m^2 for ERA 5. However, the resource grid shows a maximum power density of 224 W/m^2 for SODAR and 163 W/m^2 for ERA 5, therefore the wind farm power output can be maximized by carefully placing the turbines along the top of the hill of the plateau to take advantage of the high-power density locations.

The compressed wind streamlines near the top of the hill increase the wind speed and improve the performance of the turbines. Areas with greater power density should be given priority to optimize energy capture.

(a) 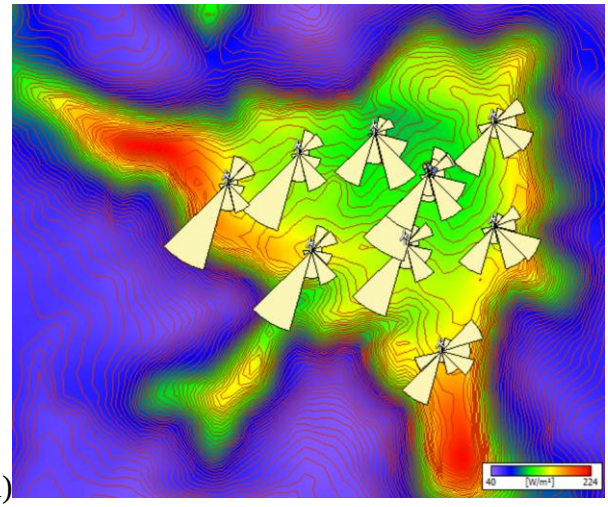 (b) 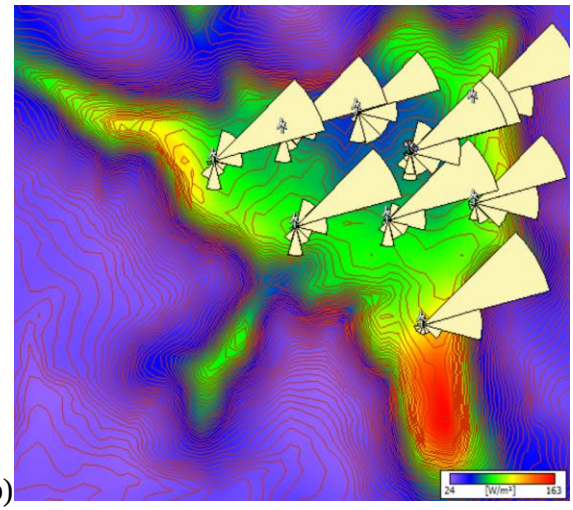

Figure 15: Resource grid with the site's power density (a) SODAR (b) ERA 5.

4.6.5. Ruggedness Index (RIX)

In WAsP, the RIX measures the impact of surface roughness on the movement of wind across the Rothe Plateau landscape. Surface roughness, which is a result from topography, affects wind speed and turbulence. RIX determines the energy capacity at different turbine sites. The resource grid in Figure 16 blue colors indicates a higher roughness index, which translates to increased surface drag and slower wind speeds while gray signifies a terrain that is smoother and has fewer surface barriers that hinder the flow of wind. This indicates that, with the reddish, pink and purple colors, the site has a reduced presence of features such as dense vegetation, structures or uneven terrain, resulting in decreased resistance to wind flow and increased wind velocities.

The RIX on the turbine site ranges from 13.3% to 16.5%. For both SODAR and ERA 5, the RIX is the same since the location is the same. This range is obtained because the topography at the turbine site is relatively uneven. The observed surface roughness indicates the existence of impediments based on the topological data from the vector map. These obstacles have a moderate impact on the flow of wind and result in reduced wind speeds. Although the terrain is not too rugged, it suggests that the wind conditions may be less stable and turbulent.

(a) 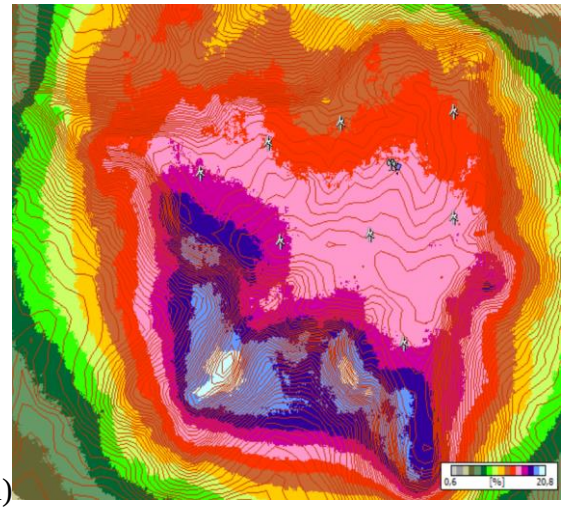 (b) 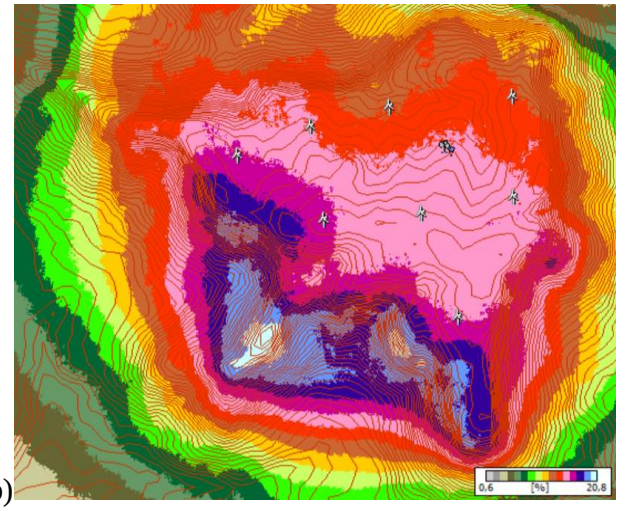

Figure 16: Resource grid displaying the Rothe Plateau's RIX (a) SODAR (b) ERA 5.

4.6.6. Turbine Placement at the Site

Across the Rothe Plateau, eight Vestas V162-6.0 MW turbines were arranged optimally, as suggested by Hirundo Lesotho. The turbines' hub heights varied from 1980.58 m to 2063.41 m above sea level and 120 m above ground level. Figure 17 shows the turbine placement on the wind resource grid using Google Earth. For SODAR, it can be seen that most of the turbines are placed in the reddish color, indicating that most of the turbines experience wind speeds that are above 5 m/s, while for ERA 5, most of the turbines are in yellowish, exposed to average wind speeds above 4 m/s. This shows that, due to the terrain of the Rothe Plateau, the turbines that will produce more power are those near the top edges or close to the hills. However, to harness the most wind out of the wind resource, the turbines can be placed at the reddish parts of the grid.

(a) 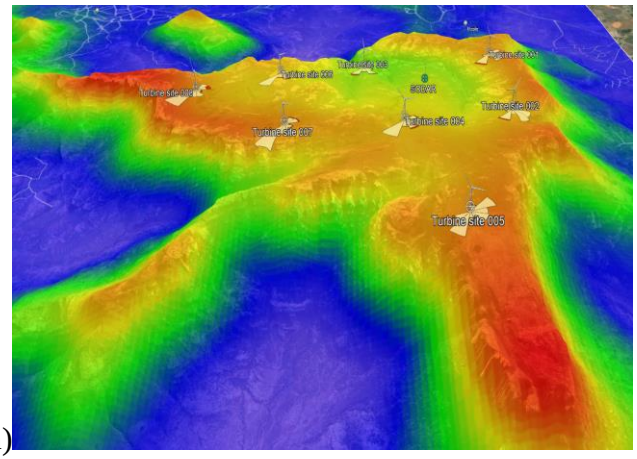 (b) 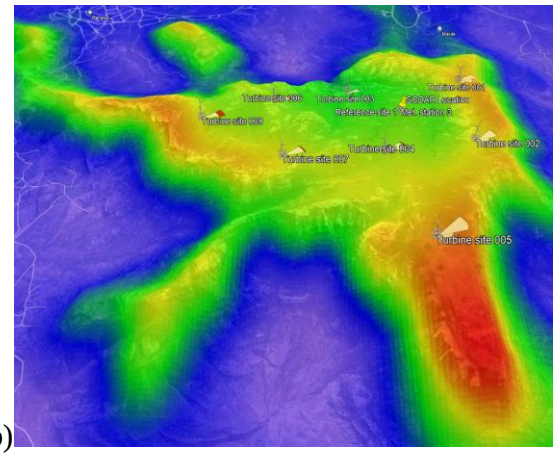

Figure 17: A Google Earth kmz file displaying the Rothe Plateau's turbine configuration (a) SODAR (b) ERA 5

As it can be seen in Figure 18, every turbine was positioned to have a separation radius three times the rotor diameter of Vestas V162-6.0 MW, which is 162 m and which guaranteed the possible spacing for minimal wake interference and effective operation. This demonstrates that the turbine blade's tip is 201 m above the ground, which is the highest point that it reaches while in a vertical orientation. This often exposes the turbine to more powerful and reliable winds that are commonly encountered at higher elevations, thereby enhancing electricity generation.

(a) 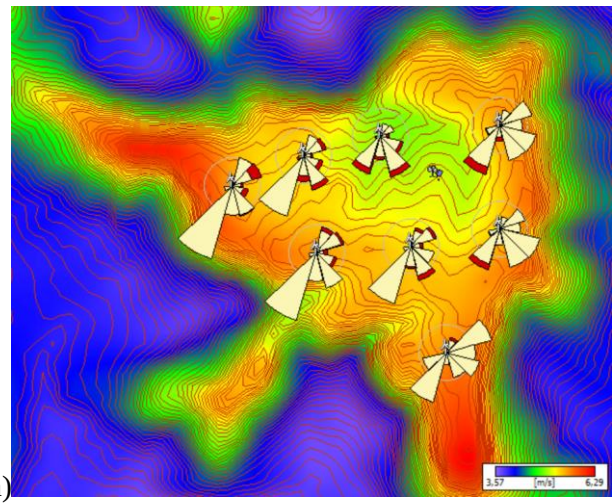 (b) 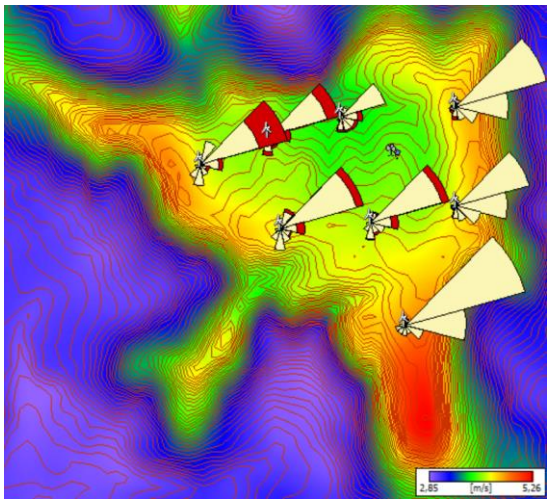

Figure 18: The resource grid is based on turbine spacing three times the crosswind rotor diameter. (a) SODAR (b) ERA 5.

4.6.7. Wind Farm Power Output

Given its 6.0 MW power output, the Vestas V162-6.0 MW turbine generator model was used for the wind farm located on the Rothe Plateau. This turbine power rating offers an effective and dependable power supply. Furthermore, the selection of the rotor diameter and tip height is optimized to enhance the capture of wind energy at the site, considering the local wind speed patterns and altitude. The wind farm has a 48 MW total output capacity with 8 erected wind turbines. Each turbine is specifically engineered to generate 6 MW of power under ideal circumstances, adding to the total energy output of the wind farm.

Table 10 displays the simulated wind farm energy production. Using the six months of data collected during the measurement campaign, WAsP was employed to examine the annual energy production (AEP) for both the SODAR and ERA 5 datasets. The SODAR instrument collected measurements at a height of 120 m, whereas the ERA 5 data was extrapolated from a height of 100 m to match the height of 120 m using WAsP. The site description, which included information about the terrain, air density and a roughness length of 0.03 m, was paired with the specs of the selected wind turbine type, Vestas V162-6.0 MW, installed at a hub height of 120 m. WAsP utilized the given inputs to determine the annual energy production (AEP) by integrating the wind speed distributions with the power curve of the turbine. Given that the data only spanned six months and assuming that the observed period accurately reflected typical annual conditions, the total annual energy production (AEP) for SODAR was found to be 75.5 GWh and 43.77 GWh for ERA 5. This demonstrates the wind farm contribution to the production of renewable energy in Lesotho, considering that the country used 848 GWh in 2022 [19]. The AEP of SODAR is higher than that of ERA 5 because SODAR uses site specific measurements as compared to the global and low-resolution ERA 5 measurements.

SODAR and ERA 5 show a wake loss of 6.62% and 8.5%, respectively. This indicates the influence of wind turbine wakes from upwind turbines. Figure 18 shows a decrease (the red color on the wind) in energy production due to the wake losses. Consequently, there is energy dissipation and an upsurge in turbulence further downstream.

Table 10: Output summary results (a) SODAR (b) ERA 5

(a)

Parameter	Total	Average	Minimum	Maximum
Net AEP [GWh]	75,477	9,435	7,170	10,913
Gross AEP [GWh]	80,827	10,103	8,115	11,093
Wake loss [%]	6,62	-	-	-

(b)

Parameter	Total	Average	Minimum	Maximum
Net AEP [GWh]	43,768	5,471	3,679	7,711
Gross AEP [GWh]	47,832	5,979	4,132	7,756
Wake loss [%]	8,5	-	-	-

Table 11 provides a study of wake effects and their effect on electricity production. Wake losses arise from the arrangement of turbines downstream, which lowers the wind speed and power production of the downstream turbines. The WAsP software was used to determine the wake losses for each turbine site. For SODAR, turbine Site 003 had the greatest wake loss percentage of 11.65% and the lowest energy production of 7.17 GWh over the six-month testing period. While ERA 5 showed that the turbine site 008 had the highest wake loss of 18.35%, turbine site 003 is the least producing turbine with 3.68 GWh. This difference in turbine wake loss for SODAR and ERA 5 is demonstrated in Figure 18 which shows different directions of the usable wind speed. Thus, for SODAR, most wind comes from the south west and the turbine site 003, being in downstream, is exposed to high wake losses, while in ERA 5 the most usable wind comes from north east, hence turbine side 008 is exposed to higher wake losses. For both SODAR and ERA 5, turbine site 003 produces the lowest annual energy because of its lowest elevation of 1,980.58 m above sea level as compared to other turbine sites that are above 2,000 m. Turbine site 005 has the lowest wake loss for both ERA 5 and SODAR and it produces the highest energy output. To maximize turbine efficiency and reduce the effects of wake interactions, turbines could be positioned at a minimum distance of 5-7 times the diameter of the rotor in the direction of the prevailing wind and 3-5 times the diameter of the rotor perpendicular to it.

Table 11: Results of each turbine site (a) SODAR (b) ERA 5

(a)

Site	Location [m]	Turbine	Elevation [m] a.s.l.	Height [m] a.g.l.	Net AEP [GWh]	Wake loss [%]
Turbine site 001	(544416,7, 6726733,0)	V162-6.0	2041,286	120	10,091	5,61
Turbine site 002	(544419,2, 6725824,0)	V162-6.0	2056,634	120	9,636	4,03
Turbine site 003	(543371, 6726639)	V162-6.0	1980,581	120	7,170	11,65
Turbine site 004	(543640,9, 6725669,0)	V162-6.0	2063,41	120	8,921	7,57
Turbine site 005	(543955,4, 6724731,0)	V162-6.0	2054,297	120	10,913	1,62
Turbine site 006	(542702,5, 6726462,0)	V162-6.0	2011,962	120	8,611	10,52
Turbine site 007	(542813,6, 6725615,0)	V162-6.0	2061,533	120	10,187	5,96
Turbine site 008	(542077,9, 6726202,0)	V162-6.0	2014,178	120	9,948	7,72

(b)

Site	Location [m]	Turbine	Elevation [m] a.s.l.	Height [m] a.g.l.	Net AEP [GWh]	Wake loss [%]
Turbine site 001	(544416,7, 6726733,0)	V162-6.0	2041,286	120	6,587	3,13
Turbine site 002	(544419,2, 6725824,0)	V162-6.0	2056,634	120	6,069	1,84
Turbine site 003	(543371, 6726639)	V162-6.0	1980,581	120	3,679	10,95
Turbine site 004	(543640,9, 6725669,0)	V162-6.0	2063,41	120	4,896	10,99
Turbine site 005	(543955,4, 6724731,0)	V162-6.0	2054,297	120	7,711	0,58
Turbine site 006	(542702,5, 6726462,0)	V162-6.0	2011,962	120	4,417	16,1
Turbine site 007	(542813,6, 6725615,0)	V162-6.0	2061,533	120	5,405	10,93
Turbine site 008	(542077,9, 6726202,0)	V162-6.0	2014,178	120	5,004	18,35

Table 12 provides a summary of the variations in shape factor and scale factor across the entire Rothe Plateau wind farm. For SODAR, the Weibull distribution model of wind speed distributions considers the shape factor ranging from 2.00 to 2.09 and the scale factor 5.6 m/s to 6.3 m/s as important factors, while for ERA 5, the shape factor ranges from 1.69 to 1.78 and the scale factors from 4.3 m/s to 5.2 m/s. Turbine site 005 is the turbine that is encountering a high average wind speed in SODAR and ERA 5, with 5.6 m/s and 4.63 m/s, respectively. The power densities for all turbine sites measured by SODAR are in the range of 109 W/m^2 to 155 W/m^2 and those of ERA 5 range from 56 W/m^2 to 109 W/m^2. ERA 5 has lower power densities than SODAR because of its low wind speeds. This is caused by ERA 5 not being able to capture the same high resolution data as SODAR and it may be due to the factors such as the fact that it does not reflect the geographical features of the Rothe Plateau well.

Table 12: Weibull and other parameters for each turbine (a) SODAR (b) ERA 5

(a)

Site	Location [m]	H [m]	A [m/s]	k	U [m/s]	E [W/m²]	RIX [%]
Turbine site 001	(544416,7, 6726733,0)	120	6,2	2,09	5,54	147	13,7
Turbine site 002	(544419,2, 6725824,0)	120	6,1	2,09	5,40	137	15,4
Turbine site 003	(543371, 6726639)	120	5,6	2,06	4,98	109	13,3
Turbine site 004	(543640,9, 6725669,0)	120	6,0	2,07	5,32	132	15,4
Turbine site 005	(543955,4, 6724731,0)	120	6,3	2,05	5,60	155	16,1
Turbine site 006	(542702,5, 6726462,0)	120	6,0	2,04	5,31	133	14,6
Turbine site 007	(542813,6, 6725615,0)	120	6,3	2,03	5,55	153	16,5
Turbine site 008	(542077,9, 6726202,0)	120	6,2	2,00	5,54	154	16,0

(b)

Site	Location [m]	H [m]	A [m/s]	k	U [m/s]	E [W/m²]	RIX [%]
Turbine site 001	(544416,7, 6726733,0)	120	5,0	1,75	4,44	92	13,7
Turbine site 002	(544419,2, 6725824,0)	120	4,8	1,76	4,30	83	15,4
Turbine site 003	(543371, 6726639)	120	4,3	1,78	3,79	56	13,3
Turbine site 004	(543640,9, 6725669,0)	120	4,6	1,76	4,14	74	15,4
Turbine site 005	(543955,4, 6724731,0)	120	5,2	1,69	4,63	109	16,1
Turbine site 006	(542702,5, 6726462,0)	120	4,6	1,75	4,08	71	14,6
Turbine site 007	(542813,6, 6725615,0)	120	4,8	1,74	4,28	83	16,5
Turbine site 008	(542077,9, 6726202,0)	120	4,8	1,72	4,28	84	16,0

4.6.8. Capacity Factor

The capacity factor quantifies the ratio of the actual output achieved during a specific time period to the highest potential output that would be obtained if the plant ran at its full capacity without interruption. To find the capacity factor, the wind farm real energy production is compared to the amount of energy that it would have produced if it had been running at its full 48 MW capacity for the whole measuring campaign. The wind farm can make almost all of its full output when the capacity factor is higher.

The designed wind farm using the on-site measurements captured by SODAR on the Rothe Plateau has a capacity factor of 17.95%, obtained using Equation 21. The low capacity factor for the Rothe Plateau is due to the insufficient wind data, which is 57.36%, resulting in inefficient power generation by the turbines. If 42.64% of the data is missing, especially during nighttime or high-wind occurrences periods, the analysis may not accurately represent the range of wind conditions and the highest wind speeds at the location. The incomplete data results in the underestimation of the wind resource, leading to a lower capacity factor. The annual average capacity factors have been demonstrated to range from 15% to 50% [80].

5. CONCLUSION

SODAR data availability collected from 23 January 2024, to 31 July 2024, after the removal of erroneous and suspicious data, was 57.36%. It is often regarded as being of poor quality because it falls below 90%. The accuracy and availability of the data determine the precision of wind resource validation. The absence of nighttime data resulted in substantial inaccuracies as wind patterns frequently vary between day and night due to temperature fluctuations and changes in atmospheric stability. Excluding the nighttime and cloudy day's data resulted in an underestimation of the total wind capacity. To enhance data capture 24/7, it would be advantageous to make a proper system size for more reliable battery solutions or alternate power backup choices. The wind rose data yielded an average wind speed of 5.1 m/s at 120 m above ground. At the turbine sites of the same height, the average wind speed ranged from 4.98 m/s to 5.60 m/s.

The wind speed distribution is further characterized by the Weibull distribution analysis, which has a scale factor *c* of 5.7 m/s and a shape factor *k* of 2.09. During the SODAR measuring campaign, February had the greatest mean wind speed (5.80 m/s). However, there is a gap in the dataset, which could result in an insufficient understanding of the wind resource because for some days the SODAR device only recorded wind speeds during the day and cloudless days due to the under sizing of the battery system. The lack of information on wind speeds at night is crucial because, depending on variables such as temperature gradients and air stability, overnight wind speeds can differ greatly from daytime wind speeds. This restriction may affect how accurately wind resources are assessed, particularly if the strength of the winds varies between day and night. The prevailing wind direction and most energy producing at the site was 60° (ENE), according to the analysis of ERA 5 data. The Weibull distribution parameters *k* and *c* were found to be 1.81 and 4.2 m/s respectively, in conjunction with the average wind speed of 3.8 m/s at 120 m above ground level.

The validity of the mesoscale ERA 5 reanalysis data was carried out with the same time series data as that of the SODAR. The coarser mesoscale grid distorts details, such as the location of the plateau; hence, to increase the accuracy and dependability of wind energy evaluations, measurements made on the ground are normally required. The correlation between SODAR and

ERA5 data for wind observations was evaluated using the correlation coefficient, the standard deviation, the mean bias error (MBE) and the normalized root mean square error (NRMSE). The correlation coefficient for wind speed was found to be 0.725 (72.5%) for the two datasets degree of linear relationship. The 72.5% correlation indicates a relatively strong and dependable association between SODAR and ERA 5. With a determination coefficient of 0.525, ERA 5 captures 52.5% of the underlying patterns in the wind data, but there is a substantial degree of unexplained variability (47.5%), which the model does not account for. This may be attributed to factors such as the local topography, where the coarser mesoscale grid fails to depict intricate details accurately. Moreover, the correlation coefficient indicated a poor connection, which was 27.7%. This is because wind direction errors are normally seen to be higher than wind errors.

The SODAR and ERA 5 datasets had a standard deviation of 1.55 m/s and 122.7^0, which measures wind speed and direction variability around the average. The NRMSE was found to be 0.122, which indicated a prediction error of 12.2% of the measured wind speed range of the SODAR data. Moreover, ERA 5 inaccurately forecasted the wind direction, which was indicated by an error of 35.9%. The mean bias error of -1.51 m/s and -7.84^0 indicates that, overall, the ERA 5 model tends to underestimate wind speeds.

Eight Vestas V162-6.0 MW turbines, placed at a hub height of 120 meters, are part of the wind farm on the Rothe Plateau that was designed using WAsP. There were no notable impediments in close proximity; hence, a roughness class of 0.03 m was employed. Approximately twenty percent (19.1%) of the wind at the turbine position, according to the wind analysis, originates from the south west, indicating that this is the major wind direction that contributes to the highest energy production.

The wind turbines on the Rothe Plateau have a high likelihood of operating effectively because of the SODAR distribution of wind speeds at turbine hub height, which range from 4.98 m/s to 5.60 m/s at a resolution of 10 meters at 120 m agl. The region consistent wind speeds point to favorable turbine operating conditions, enabling effective production of energy. The air density was determined by WAsP to be 0.95 kg/m^3. The wind speed fluctuation was measured to have a turbulence intensity of 39.4%, which signifies substantial fluctuations in wind speed, thus indicating that the wind is unstable.

The Vestas V162-6.0 MW turbine generator model was chosen for the 8 turbines, with a total capacity of 48 MW. Based on on-site SODAR data, WAsP simulated the net annual energy production of the wind farm to be 75.5 GWh, which was obtained by projecting the available data to a period of a year. The Rothe Plateau turbine arrangement low wake loss rating of 6.62% denotes less energy loss due to wake effects. Overall, the Rothe Plateau wind farm design maximizes energy output while minimizing the wake impacts. The Rothe Plateau wind farm capacity factor is 17.95%, indicating that it does not produce adequate power for its 48 MW capacity, since 30% or higher of the capacity factor signifies a substantial amount of power production. Only 57.36% of the data was collected during the six-month measurement study, which can impact annual energy production and capacity factor forecasts. Due to data shortages, the analysis may not accurately reflect wind conditions throughout the year.

To conduct a comprehensive analysis of energy production, the capacity factor and seasonal wind speed patterns at Rothe Plateau, it is necessary to have a constant measurement supply of on-site annual wind data. Furthermore, further studies could investigate larger datasets, encompassing nocturnal and seasonal fluctuations, to enhance the comparability between ERA 5 and SODAR wind observations.

REFERENCES

[1] IEA, “Renewables – Global Energy Review 2021 – Analysis.” Accessed: Sep. 26, 2023. [Online]. Available: https://www.iea.org/reports/global-energy-review-2021/renewables

[2] B. Alex, “Global Wind Report 2022,” Global Wind Energy Council. Accessed: Jul. 24, 2023. [Online]. Available: https://gwec.net/global-wind-report-2022/

[3] Statista, “Global cumulative installed solar PV capacity 2021.” Accessed: Sep. 18, 2023. [Online]. Available: https://www.statista.com/statistics/280220/global-cumulative-installed-solar-pv-capacity/

[4] UNFCC, “The Paris Agreement | UNFCCC.” Accessed: Aug. 23, 2023. [Online]. Available: https://unfccc.int/process-and-meetings/the-paris-agreement

[5] Martin, “Climate Change,” United Nations Sustainable Development. Accessed: Aug. 23, 2023. [Online]. Available: https://www.un.org/sustainabledevelopment/climate-change/

[6] Cornell University, “Wind energy can deliver a vital slash to global warming.” ScienceDaily. Accessed: Aug. 23, 2023. [Online]. Available: https://www.sciencedaily.com/releases/2021/09/210922143300.htm

[7] “Global wind power cumulative installed capacity to hit 2.38 TW in 2032,” Windpower Engineering & Development. Accessed: Nov. 4, 2023. [Online]. Available: https://www.windpowerengineering.com/global-wind-power-cumulative-installed-capacity-to-hit-2-38-tw-in-2032/

[8] S. S. Sultan and A. Gour, “Wind Power Potential Assessment of Complex Terrain at RGPV Hill Top,” *Int. J. Innov. Res. Sci. Technol.*, vol. 1, no. 10, Mar. 2015, [Online]. Available: https://ijirst.org/articles/IJIRSTV1I10009.pdf

[9] I. Baring-Gould, “WIND ENERGY DEPLOYMENT IN ISOLATED ISLANDED POWER SYSTEMS: CHALLENGES & REALITIES,” May 5, 2014. Accessed: Jun. 18, 2023. [Online]. Available: https://www.nrel.gov/docs/fy14osti/61253.pdf

[10] Lawrence Berkeley National Laboratory, “Turbine — Innovative Outcomes,” Energy I-SPARK. Accessed: Jul. 24, 2023. [Online]. Available: https://ei-spark.lbl.gov/generation/onshore-wind/turb/innov/

[11] J. Dodd, “Do we still need masts?” Accessed: Jul. 24, 2023. [Online]. Available: https://www.windpowermonthly.com/article/1458018?utm_source=website&utm_medium

=social

[12] EERE, “Wind Turbines: the Bigger, the Better,” Energy.gov. Accessed: Jul. 26, 2023. [Online]. Available: https://www.energy.gov/eere/articles/wind-turbines-bigger-better

[13] G. Xia, C. Draxl, A. Raghavendra, and J. K. Lundquist, “Validating simulated mountain wave impacts on hub-height wind speed using SoDAR observations,” *Renew. Energy*, vol. 163, pp. 2220–2230, Jan. 2021, doi: 10.1016/j.renene.2020.10.127.

[14] S. Bradley and S. Von Hünerbein, “Beam Geometry Calibration of Sodars without Use of a Mast,” *J. Atmospheric Ocean. Technol.*, vol. 30, no. 9, pp. 2161–2167, Sep. 2013, doi: 10.1175/JTECH-D-12-00112.1.

[15] S. Mokeke and L. Z. Thamae, “The impact of intermittent renewable energy generators on the Lesotho national electricity grid,” *Electr. Power Syst. Res.*, vol. 196, p. 107196, Jul. 2021, doi: 10.1016/j.epsr.2021.107196.

[16] M. Mpholo, T. Mathaba, and M. Letuma, “Wind profile assessment at Masitise and Sani in Lesotho for potential off-grid electricity generation,” *Energy Convers. Manag.*, vol. 53, no. 1, pp. 118–127, Jan. 2012, doi: 10.1016/j.enconman.2011.07.015.

[17] T. Mathaba, M. Mpholo, and M. Letuma, “Velocity and power density analysis of the wind at Letšeng-la-terae in Lesotho,” *Renew. Energy*, vol. 46, pp. 210–217, Oct. 2012, doi: 10.1016/j.renene.2012.04.003.

[18] Technical University of Denmark, “Global Wind Atlas.” Accessed: Jun. 8, 2024. [Online]. Available: https://globalwindatlas.info

[19] Lesotho Electricity and Water Authority, “Annual Report 2021-22.” Accessed: Feb. 19, 2023. [Online]. Available: https://www.lewa.org.ls/download/lewa-annual-report-2021-22/

[20] The Reporter, “Electrification of rural areas remains an issue.” The Reporter Lesotho | Fresh News, Daily. Accessed: Oct. 17, 2022. [Online]. Available: https://www.thereporter.co.ls/2022/10/05/electrification-of-rural-areas-remains-an-issue/

[21] C. Lausberg, K. Evans, and E. D. Jongh, “Effective selection of countries in sub-Saharan Africa for new market entry by independent wind power producers,” *J. Energy South. Afr.*, vol. 32, no. 4, Art. no. 4, Dec. 2021, doi: 10.17159/2413-3051/2021/v32i4a10673.

[22] Lesotho Electricity and Water Authority, “Lesotho Energy Policy 2015-2025.” Accessed: Aug. 25, 2023. [Online]. Available: https://www.lewa.org.ls/download/lesotho-energy-policy-2015-2025-2/

[23] C. Drago and A. Gatto, “Gauging energy poverty in developing countries with a composite metric of electricity access,” *Util. Policy*, vol. 81, p. 101486, Apr. 2023, doi: 10.1016/j.jup.2022.101486.

[24] S. Lang and E. McKeogh, “LIDAR and SODAR Measurements of Wind Speed and Direction in Upland Terrain for Wind Energy Purposes,” *Remote Sens.*, vol. 3, no. 9, pp. 1871–1901, Aug. 2011, doi: 10.3390/rs3091871.

[25] J. Jin, Y. Li, L. Ye, X. Xu, and J. Lu, “Integration of atmospheric stability in wind resource assessment through multi-scale coupling method,” *Appl. Energy*, vol. 348, p. 121402, Oct. 2023, doi: 10.1016/j.apenergy.2023.121402.

[26] P. K. Chaurasiya, A. K. Azad, V. Warudkar, and S. Ahmed, “Chapter 5 - Advancement in Remote Sensing of Wind Energy,” in *Advances in Clean Energy Technologies*, A. K. Azad, Ed., Academic Press, 2021, pp. 207–233. doi: 10.1016/B978-0-12-821221-9.00005-0.

[27] B. H. Bailey, S. L. McDonald, D. W. Bernadett, M. J. Markus, and K. V. Elsholz, “Wind resource assessment handbook: Fundamentals for Conducting a Successful Monitoring Program,” Apr. 1997. doi: 10.2172/486127.

[28] S. Sun, T. Wang, and F. Chu, “In-situ condition monitoring of wind turbine blades: A critical and systematic review of techniques, challenges, and futures,” *Renew. Sustain. Energy Rev.*, vol. 160, p. 112326, May 2022, doi: 10.1016/j.rser.2022.112326.

[29] K. S. R. Murthy and O. P. Rahi, “A comprehensive review of wind resource assessment,” *Renew. Sustain. Energy Rev.*, vol. 72, pp. 1320–1342, May 2017, doi: 10.1016/j.rser.2016.10.038.

[30] S. Ahmed and P. K. Chaurasiya, “Application of Remote Sensing in Wind Resource Assessment,” in *Encyclopedia of Renewable and Sustainable Materials*, S. Hashmi and I. A. Choudhury, Eds., Oxford: Elsevier, 2020, pp. 265–276. doi: 10.1016/B978-0-12-803581-8.11038-0.

[31] J. Jangid *et al.*, “Potential zone identification for harvesting wind energy resources in the desert region of India – A multi criteria evaluation approach using remote sensing and GIS,” *Renew. Sustain. Energy Rev.*, vol. 65, pp. 1–10, Nov. 2016, doi: 10.1016/j.rser.2016.06.078.

[32] F. Li, Z. Xie, Y. Yang, and X. Yu, “Investigations of synoptic wind profile patterns in complex urban areas based on LiDAR measurements,” *Build. Environ.*, vol. 242, p. 110573,

Aug. 2023, doi: 10.1016/j.buildenv.2023.110573.

[33] I. O. Ozioko, N. S. Ugwuanyi, A. O. Ekwue, and C. I. Odeh, "Wind energy penetration impact on active power flow in developing grids," *Sci. Afr.*, vol. 18, p. e01422, Nov. 2022, doi: 10.1016/j.sciaf.2022.e01422.

[34] S. Bradley, "Wind speed errors for LIDARs and SODARs in complex terrain," *IOP Conf. Ser. Earth Environ. Sci.*, vol. 1, no. 1, p. 012061, May 2008, doi: 10.1088/1755-1315/1/1/012061.

[35] P. Beaucage, G. Lafrance, J. Lafrance, J. Choisnard, and M. Bernier, "Synthetic aperture radar satellite data for offshore wind assessment: A strategic sampling approach," *J. Wind Eng. Ind. Aerodyn.*, vol. 99, no. 1, pp. 27–36, Jan. 2011, doi: 10.1016/j.jweia.2010.10.005.

[36] K. M. Prasad, G. Nagababu, and H. K. Jani, "Enhancing offshore wind resource assessment with LIDAR-validated reanalysis datasets: A case study in Gujarat, India," *Int. J. Thermofluids*, vol. 18, p. 100320, May 2023, doi: 10.1016/j.ijft.2023.100320.

[37] T. Nchaba, M. Mpholo, and C. Lennard, "Long-term austral summer wind speed trends over southern Africa," *Int. J. Climatol.*, vol. 37, no. 6, pp. 2850–2862, May 2017, doi: 10.1002/joc.4883.

[38] D. Astolfi, R. Pandit, L. Celesti, A. Lombardi, and L. Terzi, "SCADA data analysis for long-term wind turbine performance assessment: A case study," *Sustain. Energy Technol. Assess.*, vol. 52, p. 102357, Aug. 2022, doi: 10.1016/j.seta.2022.102357.

[39] J. Olauson, "ERA5: The new champion of wind power modelling?," *Renew. Energy*, vol. 126, pp. 322–331, Oct. 2018, doi: 10.1016/j.renene.2018.03.056.

[40] B. Jourdier, "Evaluation of ERA5, MERRA-2, COSMO-REA6, NEWA, and AROME to simulate wind power production over France," in *Advances in Science and Research*, Copernicus GmbH, Jun. 2020, pp. 63–77. doi: 10.5194/asr-17-63-2020.

[41] S. Von Hunerbein, I. Antoniou, H. Jørgensen, D. Kindler, and S. Bradley, "Calibration of SODARs for wind energy applications," *ResearchGate*, Mar. 2005.

[42] K. Schaldemose, "Validation of Sodar Measurements for Wind Power," in *EWEC2006: Scientific Proceedings*, Greece: EWEA, 2006. [Online]. Available: https://orbit.dtu.dk/en/publications/validation-of-sodar-measurements-for-wind-power

[43] G. Scott, D. Elliott, and M. Schwartz, "Comparison of Second Wind Triton Data with Meteorological Tower Measurements," NREL/TP-550-47429, 972514, Feb. 2010. doi:

10.2172/972514.

[44] Y. Yuechun *et al.*, "Comparison of Triton SODAR Data to Meteorological Tower Wind Measurement Data in Hebei Province, China," NREL/TP-5000-52709, 1036043, Jan. 2012. doi: 10.2172/1036043.

[45] K. S. Khan and M. Tariq, "Wind resource assessment using SODAR and meteorological mast – A case study of Pakistan," *Renew. Sustain. Energy Rev.*, vol. 81, pp. 2443–2449, Jan. 2018, doi: 10.1016/j.rser.2017.06.050.

[46] N. Kelley, B. Jonkman, G. Scott, and Y. Pichugina, "Comparing Pulsed Doppler LIDAR with SODAR and Direct Measurements for Wind Assessment," *ResearchGate*, Jan. 2007, [Online]. Available: https://www.researchgate.net/publication/237566896_Comparing_Pulsed_Doppler_LIDAR_with_SODAR_and_Direct_Measurements_for_Wind_Assessment

[47] Remtech, "Welcome - Remtech | World Leader in Acoustic Wind Profiling." Accessed: Oct. 18, 2023. [Online]. Available: https://remtechinc.com/

[48] J. Y. He, P. W. Chan, Q. S. Li, and C. W. Lee, "Characterizing coastal wind energy resources based on sodar and microwave radiometer observations," *Renew. Sustain. Energy Rev.*, vol. 163, p. 112498, Jul. 2022, doi: 10.1016/j.rser.2022.112498.

[49] S. Bradley and T. Mikkelsen, "A review of SODAR accuracy," 2012, [Online]. Available: https://backend.orbit.dtu.dk/ws/portalfiles/portal/9813117/isars2012_Bradley.pdf

[50] S. Kang *et al.*, "Wind resource assessment and potential development of wind farms along the entire coast of South Korea using public data from the Korea meteorological administration," *J. Clean. Prod.*, p. 139378, Nov. 2023, doi: 10.1016/j.jclepro.2023.139378.

[51] C. Mohrlen, J. W. Zack, and G. Giebel, *IEA Wind Recommended Practice for the Implementation of Renewable Energy Forecasting Solutions*. Elsevier, 2023. doi: 10.1016/C2021-0-03549-5.

[52] M. Optis, N. Bodini, M. Debnath, and P. Doubrawa, "Best Practices for the Validation of U.S. Offshore Wind Resource Models," NREL/TP--5000-78375, 1755697, MainId:32292, Dec. 2020. doi: 10.2172/1755697.

[53] V. Chinta, G. Song, and W. Zhang, "Validation of the medium-range and sub-seasonal forecast of solar irradiance and wind speed using ECMWF," *Energy Rep.*, vol. 10, pp.

3908–3913, Nov. 2023, doi: 10.1016/j.egyr.2023.10.058.

[54] C. Draxl *et al.*, "Mountain waves can impact wind power generation," *Wind Energy Sci.*, vol. 6, pp. 45–60, Jan. 2021, doi: 10.5194/wes-6-45-2021.

[55] J. Ramon, L. Lledó, V. Torralba, A. Soret, and F. J. Doblas-Reyes, "What global reanalysis best represents near-surface winds?," *Q. J. R. Meteorol. Soc.*, vol. 145, no. 724, pp. 3236–3251, Oct. 2019, doi: 10.1002/qj.3616.

[56] P. C. Kalverla, A. A. M. Holtslag, R. J. Ronda, and G.-J. Steeneveld, "Quality of wind characteristics in recent wind atlases over the North Sea," *Q. J. R. Meteorol. Soc.*, vol. 146, no. 728, pp. 1498–1515, 2020, doi: 10.1002/qj.3748.

[57] D. Dubov, B. Aprahamian, and M. Aprahamian, "Comparison between conventional wind measurement systems and SODAR systems for remote sensing, including examination of real wind data," in *2017 15th International Conference on Electrical Machines, Drives, and Power Systems (ELMA)*, Sofia, Bulgaria: IEEE, Jun. 2017, pp. 106–109. doi: 10.1109/ELMA.2017.7955411.

[58] J. Zhang, M. Zhang, Y. Li, J. Qin, K. Wei, and L. Song, "Analysis of wind characteristics and wind energy potential in a complex mountainous region in southwest China," *J. Clean. Prod.*, vol. 274, p. 123036, Nov. 2020, doi: 10.1016/j.jclepro.2020.123036.

[59] A. A. Shestakova, E. V. Fedotova, and V. S. Lyulyukin, "Relevance of Era5 Reanalysis for Wind Energy Applications: Comparison With Sodar Observations," *Geogr. Environ. Sustain.*, vol. 17, no. 1, Art. no. 1, Apr. 2024, doi: 10.24057/2071-9388-2023-2782.

[60] R. K. Samal, "Assessment of wind energy potential using reanalysis data: A comparison with mast measurements," *J. Clean. Prod.*, vol. 313, p. 127933, Sep. 2021, doi: 10.1016/j.jclepro.2021.127933.

[61] E. Arslan Tuncar, Ş. Sağlam, and B. Oral, "A review of short-term wind power generation forecasting methods in recent technological trends," *Energy Rep.*, vol. 12, pp. 197–209, Dec. 2024, doi: 10.1016/j.egyr.2024.06.006.

[62] M. De Lellis, R. Reginatto, R. Saraiva, and A. Trofino, "The Betz limit applied to airborne wind energy," *Renew. Energy*, vol. 127, pp. 32–40, Nov. 2018, doi: 10.1016/j.renene.2018.04.034.

[63] R. Lehneis, D. Manske, B. Schinkel, and D. Thrän, "Spatiotemporal Modeling of the Electricity Production from Variable Renewable Energies in Germany," *ISPRS Int. J. Geo-*

Inf., vol. 11, p. 90, Jan. 2022, doi: 10.3390/ijgi11020090.

[64] Z. Yang, W. Huang, S. Dong, and H. Li, "Mixture bivariate distribution of wind speed and air density for wind energy assessment," *Energy Convers. Manag.*, vol. 276, p. 116540, Jan. 2023, doi: 10.1016/j.enconman.2022.116540.

[65] J. A. Guarienti, A. Kaufmann Almeida, A. Menegati Neto, A. R. de Oliveira Ferreira, J. P. Ottonelli, and I. Kaufmann de Almeida, "Performance analysis of numerical methods for determining Weibull distribution parameters applied to wind speed in Mato Grosso do Sul, Brazil," *Sustain. Energy Technol. Assess.*, vol. 42, p. 100854, Dec. 2020, doi: 10.1016/j.seta.2020.100854.

[66] C. A. Lopez-Villalobos, O. Martínez-Alvarado, O. Rodriguez-Hernandez, and R. Romero-Centeno, "Analysis of the influence of the wind speed profile on wind power production," *Energy Rep.*, vol. 8, pp. 8079–8092, Nov. 2022, doi: 10.1016/j.egyr.2022.06.046.

[67] Y.-H. Kim and H.-C. Lim, "Effect of island topography and surface roughness on the estimation of annual energy production of offshore wind farms," *Renew. Energy*, vol. 103, pp. 106–114, Apr. 2017, doi: 10.1016/j.renene.2016.11.020.

[68] I. Inzunza-Aragón and S. E. Ruiz, "Capacity and Demand Factors Change Over Time. Application to wind turbine steel towers," *Eng. Struct.*, vol. 206, p. 110156, Mar. 2020, doi: 10.1016/j.engstruct.2019.110156.

[69] M. D'Isidoro *et al.*, "Estimation of solar and wind energy resources over Lesotho and their complementarity by means of WRF yearly simulation at high resolution," *Renew. Energy*, vol. 158, pp. 114–129, Oct. 2020, doi: 10.1016/j.renene.2020.05.106.

[70] D. Carvalho, "An Assessment of NASA's GMAO MERRA-2 Reanalysis Surface Winds," *J. Clim.*, vol. 32, no. 23, pp. 8261–8281, Dec. 2019, doi: 10.1175/JCLI-D-19-0199.1.

[71] C. Draxl *et al.*, "The Verification and Validation Strategy Within the Second Wind Forecast Improvement Project (WFIP 2)," 2019, Accessed: Nov. 6, 2023. [Online]. Available: https://www.academia.edu/79242172/The_Verification_and_Validation_Strategy_Within_the_Second_Wind_Forecast_Improvement_Project_WFIP_2_

[72] J. W. Messner, P. Pinson, J. Browell, M. B. Bjerregard, and I. Schicker, "Evaluation of wind power forecasts—An up-to-date view," *Wind Energy*, Jan. 2020, doi: 10.1002/we.2497.

[73] J. Yan, C. Möhrlen, T. Göçmen, M. Kelly, A. Wessel, and G. Giebel, "Uncovering wind

power forecasting uncertainty sources and their propagation through the whole modeling chain," *Renew. Sustain. Energy Rev.*, vol. 165, p. 112519, Sep. 2022, doi: 10.1016/j.rser.2022.112519.

[74] D. Entekhabi, R. Reichle, R. Koster, and W. Crow, "Performance Metrics for Soil Moisture Retrievals and Application Requirements," *J. Hydrometeorol.*, vol. 11, Jun. 2010, doi: 10.1175/2010JHM1223.1.

[75] H. Yizhaq, Z. Xu, and Y. Ashkenazy, "The effect of wind speed averaging time on the calculation of sand drift potential: New scaling laws," *Earth Planet. Sci. Lett.*, vol. 544, p. 116373, Aug. 2020, doi: 10.1016/j.epsl.2020.116373.

[76] Copernicus Knowledge Base - ECMWF Confluence Wiki, "ERA5: How to Calculate Wind Speed and Wind Direction from U and V Components of the Wind?" Accessed: Mar. 25, 2024. [Online]. Available: https://confluence.ecmwf.int/pages/viewpage.action?pageId=133262398

[77] J.-L. Song, J.-W. Li, R. G. J. Flay, A. A. S. Pirooz, and J.-Y. Fu, "Validation and application of pressure-driven RANS approach for wind parameter predictions in mountainous terrain," *J. Wind Eng. Ind. Aerodyne.*, vol. 240, p. 105483, Sep. 2023, doi: 10.1016/j.jweia.2023.105483.

[78] D. Koracin *et al.*, "Tall Tower Wind Energy Monitoring and Numerical Model Validation in Northern Nevada," NREL/SR--5000-62894, 1225900, Oct. 2015. doi: 10.2172/1225900.

[79] U. Yılmaz, F. Balo, and L. S. Sua, "Simulation Framework for Wind Energy Attributes with WAsP," *Procedia Compute. Sci.*, vol. 158, pp. 458–465, Jan. 2019, doi: 10.1016/j.procs.2019.09.076.

[80] A. Boretti and S. Castelletto, "Cost of wind energy generation should include energy storage allowance," *Sci. Rep.*, vol. 10, no. 1, p. 2978, Feb. 2020, doi: 10.1038/s41598-020-59936-x.